CRACK GROWTH MEASUREMENT AND FRACTURE TOUGHNESS OF PLAIN CONCRETE BEAMS

by

GARY LEE JONES

B. S., Kansas State University, 1976

A MASTER'S THESIS

submitted in partial fulfillment of the

requirements for the degree

MASTER OF SCIENCE

Department of Civil Engineering

KANSAS STATE UNIVERSITY
Manhattan, Kansas

1982

Approved by:

Major Professor

Table of Contents

Table of Contents Con't.

List of Tables

List of Figures

List of Figures Con't.

Page

CHAPTER I

Introduction

Determination of crack length is the first major step in observing the effects cyclic loading has on structural concrete. Generally, crack widths are so small that unaided observations are not reliable. Therefore, in order to accurately relate the rate of crack growth to the fatiguing process a reliable means of crack length measurement must be established. The purpose of this thesis is to examine four of the available experimental methods for measuring crack length and, using the most successful method, monitor crack growth in beam specimens subjected to cyclic loading. Results from the fatiguing process are then used to determine the fracture toughness of the specimen.

This thesis will be divided into six major parts: (1) review of literature, (2) test equipment, (3) mix design, (4) experimental methods for determining crack growth, (5) tests on plain concrete beams, and (6) conclusions.

CHAPTER II

Review of Literature

Fracture mechanics concepts have been successfully employed in determining the failure of metallic structural members when subjected to either static loading or cyclic loading. Fracture mechanics has also been used successfully by Schmidt (5) in his research into the fracture toughness of limestone.

Schmidt (5) found that compliance calibration provided a reliable means of measuring crack length in limestone beams and subsequently, used it to obtain data for the determination of the fracture toughness of limestone. Test results for limestone indicate that the fracture toughness does not depend on the orientation of the cracks in relationship to the bedding plane. Also, Schmidt (5) noted that fracture toughness tends to increase with an increase in specimen size and crack length. During his tests Schmidt (5) observed that cracks in specimens closed upon removal of the load.

Concrete differs from metals and limestone in that, it is a heterogeneous, inelastic material. This fact creates difficulties in the application of fracture mechanics to concrete since crack propagation will be dependent on a combination of bond, aggregate and mortar failure.

Glücklich (2) noted that concrete behaves like glass in that, strain-energy for both materials is transformed into primarily surface tension. However, concrete also differs from glass because it is heterogeneous. The heterogeneity of concrete allows for the formation of a zone of microcracks in place of a single crack, as in the

case of glass. Glücklich (2) observed that, as a crack grows, the zone of microcracks is increased and a corresponding increase in load is required to cause further crack propagation. The propagation of a crack through the concrete is a result of three types of failure working interdependently to form the network of cracks which leads to ultimate failure of the specimen.

The most common type of failure, as observed by Glücklich (2), was that of the bond between the aggregate and cement gel. Cracks would proceed around the aggregate until a higher level of stress was required. At that time the crack would be arrested. Crack propagation could continue when the stress exceeds the bond stresses or, as in the case of the second type of failure, the stress exceeds the strength of the cement gel. When the strength of the cement gel is exceeded the crack no longer follows the face of the aggregate but proceeds through the cement gel, thus increasing the total surface area of the crack. The entire process occurs continuously but is a system of interrelated crack formations, propagations, arrests, and formation of new cracks or continuations of existing cracks until the specimen ultimately fails.

The third type of failure is the fracture of the aggregate. Glücklich (2) stated that this form of failure rarely occurred and was possibly dependent on the type of aggregate used. He did note however, that aggregate size had a definite influence on the strength of concrete. With larger aggregate the crack must penetrate the sand-cement matrix less often and since the bond strength is less than that

of the matrix the overall strength is reduced.

Naus and Lott (4), report results of an experimental study using notched beam specimens to obtain values of the "effective fracture toughness" for concrete. They examined the effects of water-cement ratio, air content, curing time, fine aggregate content and gravel content on the values of the "effective fracture toughness."

Naus and Lott (4) noted that, for mortar and cement series, with an increase in water-cement ratio, there is a decrease in the effective fracture toughness. They also noted that this decrease is not apparent in concrete. This probably occurs because the effects of aggregates as crack arresters are more significant than the effect the water-cement ratio has in reducing the effective fracture toughness of the paste matrix. The crack arresting ability of the aggregate also appeared to successfully offset the reduction of the effective fracture toughness caused by increasing the air content of the concrete.

Naus and Lott (4) reported that effective fracture toughness increased with age. This increase was attributed to the continued hydration of the cement which resulted in increased matrix strength. While curing time tended to increase the effective fracture toughness the investigators noted that after 90 days increases were insignificant because of the decrease in rate of hydration with time.

Fine aggregate tended to increase the effective fracture toughness of mortar. However, Naus and Lott (4) reported that this increase was not apparent in concrete because of the overriding effect of the coarse aggregate. The effective fracture toughness was found to be increased

by both the increase in coarse aggregate particle size and the increase in the quantity of coarse aggregate in the concrete. In the former case a maximum size limit was noted by Naus and Lott (4), beyond which the effective fracture toughness was lowered because of the effect of segregation. The increase in effective fracture toughness which results from the presence of coarse aggregate can be attributed to the aggregate's effectiveness as a crack arrester.

Shah and McGarry (6) investigated the applicability of Griffith fracture criterion to portland cement paste, mortar, and concrete. They found that the cement paste is a notch sensitive material. The tensile and flexural strength is significantly reduced by the introduction of a notch into a paste specimen. This notch sensitivity of paste appears to be governed by the Griffith fracture criterion.

Shah and McGarry (6) noted that, while cement paste is notch sensitive, mortar and concrete appear to be notch insensitive. The fracture of these materials occurs at a stress level similar to the level present in unnotched specimens. The process of stable crack growth will continue until a critical crack length is reached. Shah and McGarry (6) observed that, at that point crack propagation is likely to be spontaneous and at that time the Griffith fracture criterion may be applicable to mortar and concrete. The investigators stated that microcracks less than a critical length will undergo gradual and stable growth until the critical length is reached. The critical length will probably depend on the nature and volume of the aggregate with larger volumes and greater size aggregates resulting in larger critical crack

lengths.

Shah and McGarry (6) concluded that the failure of concrete is the result of progressive deterioration rather than the unstable growth of one crack.

CHAPTER III

Test Equipment

Vishay Data Acquisition System

The Vishay Data Acquisition System shown in Figure 1 was used to monitor strain gage output from tension and compression tests. The system has fifty channels which can be used in either quarter-, half-, or full-bridge configurations. Besides a digital display of strain the Vishay System is capable of providing constant strain printout of one channel per second with an accuracy of $\pm$ 1 $\mu\epsilon$.

Test Fixture for Tension Specimen

To determine whether or not Young's Modulus varies from tension loading to compression loading it was necessary to develop some method for testing a cylinder directly in tension. The values of Young's Modulus and the ultimate strength, f_t', provided by this method could also be used in a finite element computer program for the determination of the theoretical fracture toughness of concrete.

Figure 2 shows the jig that was used to mount the cylinders in place. The jig is the same type as that used to cap compression cylinders. The cylinders were held in place by Sika Dur High Mod Gel which has a tensile strength of approximately 5,000 psi (34,457 KN/m^2). The gel provided adequate strength for tension tests and was also easy to remove from the fixture by heating the fixture to approximately 300°C.

During the mounting process it is generally not possible to align a specimen in a manner that would minimize load eccentricities. Figure 3 shows the apparatus that was emplcyed on the tension fixture

for minimizing these eccentricities. With a slight load on the specimen the adjustment screws were turned until all strain gage readouts were at a minimum. The assembled fixture with a failed specimen can be seen in Figure 4.

MTS Model 903.32

The MTS system was used for all compliance calibration tests. The system was also used for fatigue precracking and load to failure tests. The MTS is a closed-loop, electrohydraulic loading system capable of operation in either load, stroke, or strain control. During the fatiguing process the MTS was operated in the stroke control mode and, for compliance measurement load control was used. The load range used for all experiments was ± 10,000 lbs. (± 44,500N) since it was the lowest load range of the MTS system. The MTS system also provided a linear relationship between voltage output and applied load. The relationship was 1,000 lbs. (4,450N) resulted in a one volt output. In addition to using the load indicator during testing, voltage was also monitored to provide verification of loads applied to beam specimens. A view of the testing system can be seen in Figure 5.

Since the lower portion of the load range was used for all tests its sensitivity was calibrated using a Schaevitz load cell and strain readout device. The load cell had a sensitivity of 600 counts per 100 lbs. (455N) of load. Using this device it was possible to calibrate the Y-axis of the MTS plotter to a sensitivity 6.16 lbs. per cm. (24.41N per cm). The calibration allowed a sufficiently accurate

measurement of failure loads which ranged from approximately 75 lbs. (334N) to 280 lbs. (1246N).

Beam Test Fixture

The basis for design of the beam test fixture was taken from recommendations set forth in ASTM 399T, which specifies procedures for fatigue testing. The design followed ASTM tolerances but was modified to work with beams formed in available molds. A drawing of the fixture and specimen can be seen in Figure 6. The rollers were held in place by rubber bands which also allowed them to move freely as the specimen deflected. The notch in the center of the fixture allowed room for a crack opening displacement gage to be mounted to the beam.

CHAPTER IV

Mix Design

In the design of the concrete mix it was desired to have a short curing time and an ultimate strength, f_c', of 3,000 psi (20,685 KN/m^2). The short curing time was obtained by using Type III Portland Cement.

To achieve an f_c' of 3,000 psi (20,685 KN/m^2), five test batches were made using different water-cement ratios as a basis for the mix designs. Using the compression test results, the curve of f_c' vs. water-cement ratio shown in Figure 7 was constructed. The final mix design was obtained by entering the curve with 3,000 psi (20,685 KN/m^2) and finding the corresponding water-cement ratio. The composition of the final mix design can be seen in Table 1.

Using the final mix design twenty-four 3 in. x 4 in. x 16 in. (7.62 cm x 10.16 cm x 40.64 cm) beam specimens and thirty 3in. x 6 in. (7.62 cm x 15.24 cm) test cylinders were cast. Although the beams were not in strict conformity to those recommended by ASTM the dimensions were used because steel forms were available.

Stabilization of f_c' was considered vital since the fatigue testing was to cover an extended period of time and variation might significantly influence test results. For this reason, compression tests were run daily for fifteen days to monitor f_c'. The 7-day value of f_c' was approximately 3,000 psi (20,685 KN/m^2) and maximum stabilization occurred with an f_c' of 5,200 psi (35,854 KN/m^2).

During the fifteen day period of compression tests three compression specimens with BLH electronic resistance wire strain gages attached

(A5-1-S6) were loaded to failure while strains were being monitored. Three strain gages were attached parallel to the longitudinal axis and approximately 120° apart. These gages were used to plot a stress vs. strain curve for determination of Young's Modulus in compression. Figures 8 and 9 show the individual stress-strain relationships for cylinders #2 and #3 respectively, and Figure 10 shows the average stress-strain relationship for the two cylinders. Prior to the load to failure test of the compression cylinders all specimens were cycled from zero to a maximum load of 5,000 lbs. (22,240 N) to minimize drift in the strain gages. Generally, five cycles were adequate to stabilize the gages.

In addition to the longitudinal strain gages, two gages were mounted perpendicular to the longitudinal axis of the cylinders. The strains recorded by these gages were used along with strains from the longitudinal gages to determine Poisson's Ratio for future use in a finite element program. The plot of stress vs. Poisson's Ratio can be seen in Figure 11. As can be seen in Figure 11, there is little variation between cylinders in the mid-ranges however, there is some scattering of results at both high and low stress levels.

Two cylinders were also tested in direct tension. These tension specimens also had five BLH wire strain gages (A5-1-S6) attached for monitoring strains. Three of the gages were mounted to record axial strain and two were mounted to record radial strain. The specimens were cycled from zero to 500 lbs. (2224 N) to minimize drift in the strain gages. Generally, five cycles were adequate to stabilize the gages.

The results of the tension tests were used to determine Poisson's Ratio and Young's Modulus for later use in a finite element computer program. Figures 12 and 13 show the relationships between tensile stress and strain for tension cylinders #1 and #2 respectively, and Figure 14 shows the average for the two cylinders. The relationship between Poisson's Ratio and tensile strength can be seen in Figure 11.

In addition to the determination of Young's Modulus in tension, the tension tests also provided an accurate estimation of the ultimate tensile strength of the final mix design. This information, along with the formula,

$$P = \frac{\sigma b(d-c)^2}{1.5\ L} \qquad (1)$$

which was derived from the formula for the Modulus of Rupture, was used to determine the maximum load to be applied to the specimen during fatigue testing. In Equation (1) the terms are defined as follows:

P = load corresponding to stress ($=f_t'$) applied at center of beam with span L;

b, d = width and depth of the beam respectively;

c = overall depth of edge crack and notch.

The maximum load was then reduced by 50% to provide an additional factor of safety against premature failure of fatigue specimens.

Consistencies in results, as indicated in the figures, showed that, although there was some deviation, the methods used were within usual experimental error. As an example, the value of Young's Modulus,

determined experimentally, is in substantial agreement with that value determined using the American Concrete Institute formula,

$$E_c = 33w^{3/2}\sqrt{f_c'} \qquad (2)$$

which yields a value of 3.65×10^6 psi (2.52×10^7 KN/m^2) for Young's Modulus. In this formula W is the unit weight of concrete (pcf) and f_c' is the ultimate strength in compression (psi).

A summary of the properties for all tension and compression cylinders can be seen in Table 2.

CHAPTER V

Experimental Methods for Determining Crack Growth

In order to verify actual crack lengths in fatigue specimens several methods of crack length measurement were tried to determine their applicability. These were: photoelasticity, foil crack propagation gages, visual inspection, MTS displacement gage (MTS Model 932.05), and compliance measurements.

Beam Pre-notching

All specimens were notched at mid-span with a commercially available masonry saw. The notch width was 0.13 in. (3.30mm) and the notch tip was essentially flat. The notching technique was the same for both the compliance calibration specimens and the fatigue specimens. Notch depths did, however, vary for the calibration specimens.

Photoelasticity

Two photoelastic sheets (Photolastic Part No. PS-2A) 0.12 in. (3mm) thick were attached to both sides of a pre-notched beam at mid-span. Photolastic PC-1 adhesive was used as the bonding agent. On one side, the sheet was left solid and, on the other side, a notch of the same configuration as that in the beam was cut. The beam was then placed in the load frame and a static load was applied so a constant fringe pattern could be observed on the photoelastic sheet. The load was gradually increased so that the crack formed and began to propagate.

The photoelastic sheet showed the stress concentrations at the root of the crack clearly and also showed the dissipation of strain away from

the crack as shown in Figure 15. Difficulty arose however, because, as shown in Figure 16, the sheet provided reinforcement which prevented proper crack formation. Note the difference in the surface between the beam section on the left (without the plastic sheet) and the one on the right. Since the possibility of reinforcing action existed, the prospect of using photoelasticity as a means of determining crack growth was abandoned.

Crack Propagation Gages

One crack propagation gage (Micro-Measurements Part No. TK-09-CP C03-003/s) 1.56 in. x 0.75 in. x 0.0017 in. (3.96 cm x 1.90 cm x 0.0043 cm) was attached, following surface preparation, to a pre-notched beam on one side, at mid-span using Eastman 910 adhesive. The gage was placed in such a manner that it rested at the root of the notch as shown in Figure 17. The specimen was then placed in the load frame and loaded while the resistance in the gage was monitored to determine crack growth.

At the present time, there is some doubt as to whether or not these gages will work satisfactorily. It was difficult to maintain an adequate bond between the gage and concrete but, if this problem can be overcome the crack gage should provide a suitable method of monitoring crack growth. Note should be made at this point that, unlike the photoelastic sheets, the crack propagation gages provided no apparent reinforcing action.

Visual Inspection

One of the most successful methods used for monitoring crack growth was visual inspection. Inspection was made utilizing a hand held magnifying glass equipped with an internal light. The method yielded results

that were within approximately 0.05 in. (1.27mm) of the results obtained from compliance measurement which will be discussed next.

While visual inspection yielded results which appeared to be accurate, its use as the sole means of determining crack growth would be difficult to justify. The method in general relies on the judgement of the observer and results could possibly vary from observation to observation and specimen to specimen.

Compliance

Compliance measurement involves the testing of beams with various notch lengths to determine the relationship between crack-opening-displacement (C.O.D.) and applied load. All beams were notched as previously described. The C.O.D. was monitored using a commercially available displacement gage (MTS Model 932.05). The gage was a cantilever beam and was used to measured displacements normal to the notch which were linearly proportional to voltage changes. In the most sensitive range 1 volt represented 0.0002 in. (5.08×10^{-3}mm). Using this range to calibrate the X-axis of the MTS system plotter, the maximum crack-opening-displacement sensitivity achieved was 7.36×10^{-6}in. per cm (18.69×10^{-6}cm per cm) of chart. The compressed gage length was 1.04 in. (2.64 cm).

The procedure, as described by Schmidt (5), for compliance testing of beams involved the following steps:

1.) Cut a notch at mid-span. This was done as previously discussed. The initial notch was shallow and for each successive test the depth of the notch was increased.

2.) Mount the knife edges for the displacement gage. Initially this was accomplished using Duco Cement and, while there was no creep once the cement hardened, the time required for hardening made the method undesirable. A minimum of 24 hours was required before the glue provided sufficient stability for testing.

As shown in Figure 18 a subsequent method was developed whereby the knife edges were clamped on. This method was extremely accurate since the edges could easily be adjusted and the total time required for the knife edge installation was 5-10 minutes.

3.) Once the knife edges were in place and the gage attached, the beam was placed in the load frame and a load applied. The load was applied at a rate of approximately 3.0 lb./sec. (13.4 N/sec.) and this resulted in a C.O.D. of approximately 0.3×10^{-4} in./sec. (7.6×10^{-5} cm/sec.). The load was cycled between zero and a maximum several times before any plot was made. Then three plots of load-C.O.D. were made and an average of the three computed. The measured slope of the three plots deviated from the average by no more than approximately ±2% for all beams and notches tested.

The variation of beam stiffness can be seen in Figure 19. The steepest slope represents a notch length of approximately 0.65 in. (1.65 cm) and the load sustained was approximately 100 lbs. (445 N). The flattest slope represents a notch length of approximately 3.12 in. (7.92 cm) in a beam 4 in. (10.16 cm) deep. The load sustained by this

beam was approximately 5 lbs. (22N.) and, with the MTS in stroke control it was possible to apply this load without subsequent failure of the beam.

Figure 20 shows the curve used in subsequent tests to determine crack length. This curve is a plot of crack length to beam depth, a/D vs. Compliance, C; compliance being taken as the inverse slope of the load-displacement curves shown in Figure 19. In Figure 20 is also shown the theoretical values of compliance obtained from finite element analysis utilizing the average material properties listed in Table 2. The deviation of experimental values, for higher compliances and for the purpose of estimating crack length, may be taken as 9% for a given compliance. This deviation is probably caused by: (1) the inherent variability of concrete material properties; and (2) the variability of attaching knife edges to the specimen.

CHAPTER VI

Tests on Plain Concrete Beams

Precracking of Beams by Fatigue

A total of eight beams were precracked. Each beam was pre-notched using methods previously described. The notches averaged 0.4 in. (10mm) in depth with minor variations occurring between beams.

After notching, the beams were placed in the test fixture shown in Figure 6 and the fixture was then mounted in the MTS load frame shown in Figure 5. Using the MTS system in stroke control a sinusoidal loading of 4 Hz was applied to the specimen. The load range of beams 1-6 varied from approximately 100 lbs. (445 N) to a maximum of approximately 900 lbs. (4,005 N.), the resulting stress range was approximately 460 psi (3,174 kN/m^2).

As shown in Table 3 the total number of load cycles varied considerably for different beams. Beams 2-6, and 8 were loaded until the total crack length, including the notch, was approximately 3 in. (7.62cm). Total cycles for beam 5 was 230 and beams 2 and 6 were cycled between 10,000 and 15,000 times. In the case of beams 3 and 4 the crack length occurred almost immediately upon application of the load. Due to the lower stress level for beam 7 crack formation did not occur until approximately 15,000 cycles. At that time a crack was noted but propagation did not occur until 26,241 cycles. A crack approximately 0.89 in. (2.26cm.) formed in beam 1 at 8,000 cycles and loading was terminated at that point. Subsequently all beams except 1 and 7 were loaded to failure.

Compliance and Failure of Cracked Beams

After all of the beams had been cracked by fatigue, compliance tests were performed as previously discussed. Once the compliance was determined it, along with the compliance curve in Figure 20, was used to find the crack length.

During the compliance testing it was desired to know if the crack closed after the load was removed. This phenomenon was typical in the limestone beam tested by Schmidt (5). In Figure 21 two load-C.O.D. curves for beam 7 are shown. Curve A represents a crack with a length of 0.67 in. (1.70cm.) which was recorded at 20,861 cycles. Curve B represents a crack with a length of 0.81 in. (2.06cm.). Note that both curves are linear and there is no noticeable change in slope which would indicate a change in beam stiffness. Refer now to Figure 22 which is a load-C.O.D. curve for beam 5. Note that in this figure there are two distinct slopes to the curve. The initial slope represents the time when the crack is closed and the beam stiffer, hence, the steeper slope. The decreased slope on the latter part of the curve indicates that the crack has opened and the beam stiffness has decreased.

The applicability of compliance measurement as a means of determining crack length in plain concrete is typified in Figure 23. The curve shown indicates the slow but constant increase of crack length in a beam subjected to cyclic loading. As shown in this figure, a rapid extension of the crack length occurred at 140,000 cycles at which time the experiment was terminated. The total crack length at this point was 3.3 in. (8.4cm.).

As was stated earlier, visual inspection was considered to be a viable means of determining crack length and propagation. Figure 24 is a photograph of beam 1 after 8,000 cycles, note the horizontal mark in the upper left hand corner. This mark represents the upper limits of crack propagation as determined by visual inspection. The crack in Figure 24 has extended approximately 0.5 in. (1.27cm.) from the notch. Subsequent compliance testing verified the visual observation made on beam 1.

A load-to-failure curve for beam 6 can be seen in Figure 25. The shape of the curve is typical for all beams. The lack of a change in slope of this curve tended to indicate that the crack remained open and, for that reason the initial slope was used to determine the compliance and crack length for this beam.

There was some concern regarding the mode of failure of the test specimen. That is, was failure due to bond failure between the aggregate and the mortar mixture or, was failure due to the fracture of the aggregate? Figure 26 shows a typical failure surface and as shown the failure appeared to be random in nature with bond failures occurring in some locations and aggregate fracturing in others.

Fracture Toughness of Plain Concrete

The fracture toughness was determined theoretically using a finite element program* shown schematically in Figure 27 and experimentally using methods established by ASTM (1). Both theoretical and experimental values of the fracture toughness for several specimens can be seen in Table 4.

---

* Developed at Kansas State University by Dr. K. K. Hu and J. Huang - see Ref. 3.

Theoretical Fracture Toughness

The finite element program (3) used an internal rectangular mesh to simulate the conditions that exist in a specimen as a load is applied. The program is initiated by inputting material, geometrical, and load data. The mesh is then generated and a stiffness matrix established for each element in the matrix. The program then establishes the initial boundary conditions and using these determines the stiffness of the beam and the resulting displacement. At this point the program determines the stress-intensity in the region of the crack tip.

Experimental Fracture Toughness

Experimental methods suggested by ASTM (1) were used to determine beam failure loads for use in calculation of the fracture toughness K_c. The failure load, P_q, was determined by extending a line, with a slope of 95% of the initial slope, to the point where it intersects the load-to-failure curve. The load at that point is taken to be the failure load. In the case of beam 5, where there was an indication of crack closure, the initial slope was taken as the slope of the curve after the crack opened. Figure 25 shows a typical load-to-failure curve and also shows the method of determining the failure load. Table 4 summarizes failure loads and fracture toughness values that were determined theoretically and experimentally.

CHAPTER VII

Conclusions

Based on research for this thesis the following conclusions are made.

1.) Direct tension testing of plain concrete is possible and it is possible to obtain consistent, accurate results repeatedly.

2.) Photoelasticity is not suitable as a means of monitoring crack growth in plain concrete beams.

3.) Crack propagation gages may provide a suitable means of monitoring crack growth however, more experimentation is needed to verify this.

4.) Visual inspection used in conjunction with other methods can be used to estimate crack length in plain concrete beams.

5.) Compliance measurement is the most suitable and convenient method for monitoring crack growth in plain concrete.

6.) Crack growth can be controlled during the fatiguing process and loading terminated before beam failure.

7.) Crack closure upon removal of the load does not appear to be consistent. This may be due to a shift in position of the aggregate particles or a relative shift in the crack surfaces.

8.) Beam failure does not result exclusively from either bond failure or aggregate fracture, but is a combination of both.

The distribution of these failure mechanisms appears to be random in nature and is independent of the particle size.

9.) Fracture toughness may not be a significant material property of concrete. However, it may become significant when it is related to aggregate size, gradation, and mix proportion.

LIST OF TABLES

Table 1: FINAL MIX DESIGN

Cement: Type III

Water/Cement Ratio: 0.80

Slump: 3 in.

Sand: S.G. = 2.49

F.M. = 3.20

Aggregate: 3/8 in. minus, well-graded

Unit weight = 96.9 lb./ft.^{3}

S.G. = 2.50

Unit Weight of Mix: 133 lb./ft.^{3}

3 in. x 6 in. cylinders used for direct tension and direct compression tests.

Table 2 Material Properties of Concrete Cylinders

Load Type T = Tension C = Compression	Failure Stress psi (kPa)	Secant Modulus of Elasticity . psi x 10^6 (kPa x 10^6)	Poisson's Ratio
C	6000 (41400)	3.65 (25.18)	0.19
C	5380 (37122)	3.27 (22.56)	0.14
C	5660 (39054)	3.52 (24.29)	0.16
T	495 (3416)	3.84 (26.50)	0.18
T	422 (2912)	3.70 (25.53)	0.18

Table 3: Measured Crack Lengths of Fatigue Loaded Beams

Specimen	Crack Length, in. (cm.)		Fatigue Cycles
	Surface Measurement	Compliance Measurement	
1	0.92 (2.34)	0.89 (2.26)	8,000
2	3.10 (7.87)	3.24 (8.23)	14,520
3	3.25 (8.26)	3.04 (7.72)	0
4	3.06 (7.77)	3.30 (8.38)	0
5	2.70 (6.86)	2.90 (7.37)	230
6	3.30 (8.38)	3.15 (8.00)	14,200
7	0.53 (1.35)	0.67 (1.70)	20,891
7	0.75 (1.90)	0.81 (2.06)	26,241
8	-	3.30 (8.38)	151,206

Table 4: Effective Fracture Toughness of Precracked Beams

Specimen	Final Crack Length (1) Inches (cm)	Load Cycles	P_q lbs. (N)	K_c psi $\sqrt{in.}$ ($KNm^{3/2}$)	
				F.E. Program	Brown and Srawley (1)
1	0.89[2] (2.26)	8,000	136[2] (605)	97[2] (107)	105[2] (115)
2	3.24 (8.23)	14,520	101 (449)	606 (667)	573 (629)
3	3.04 (7.72)	0	155 (690)	716 (788)	704 (772)
4	3.30 (8.38)	0	76 (338)	479 (527)	461 (508)
5	2.90 (7.37)	230	167 (743)	618 (680)	652 (715)
6	3.15 (8.00)	14,200	284 (1264)	1548 (1703)	1458 (1600)
7	0.81[2] (2.06)	26,241	167[2] (743)	114[2] (149)	122[2] (134)
8	3.30 (8.38)	151,206	114 (507)	718 (790)	692 (759)

1. Based on compliance measurement using slope of curve after crack opened.
2. Specimen was not loaded to failure-P_q was highest measured load. These values represent stress-intensity factors.

LIST OF FIGURES

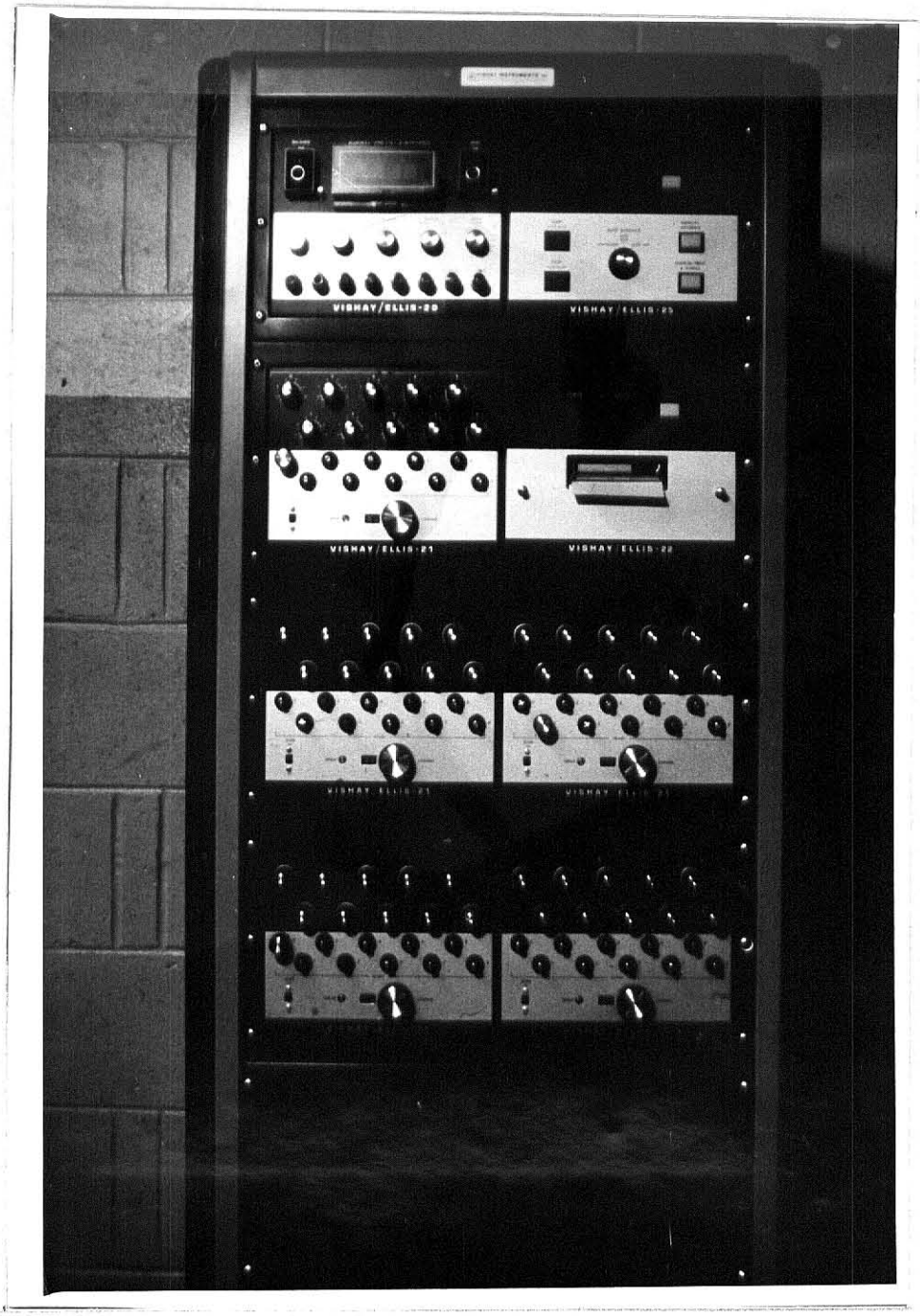

Figure 1. Vishay Data Acquisition System

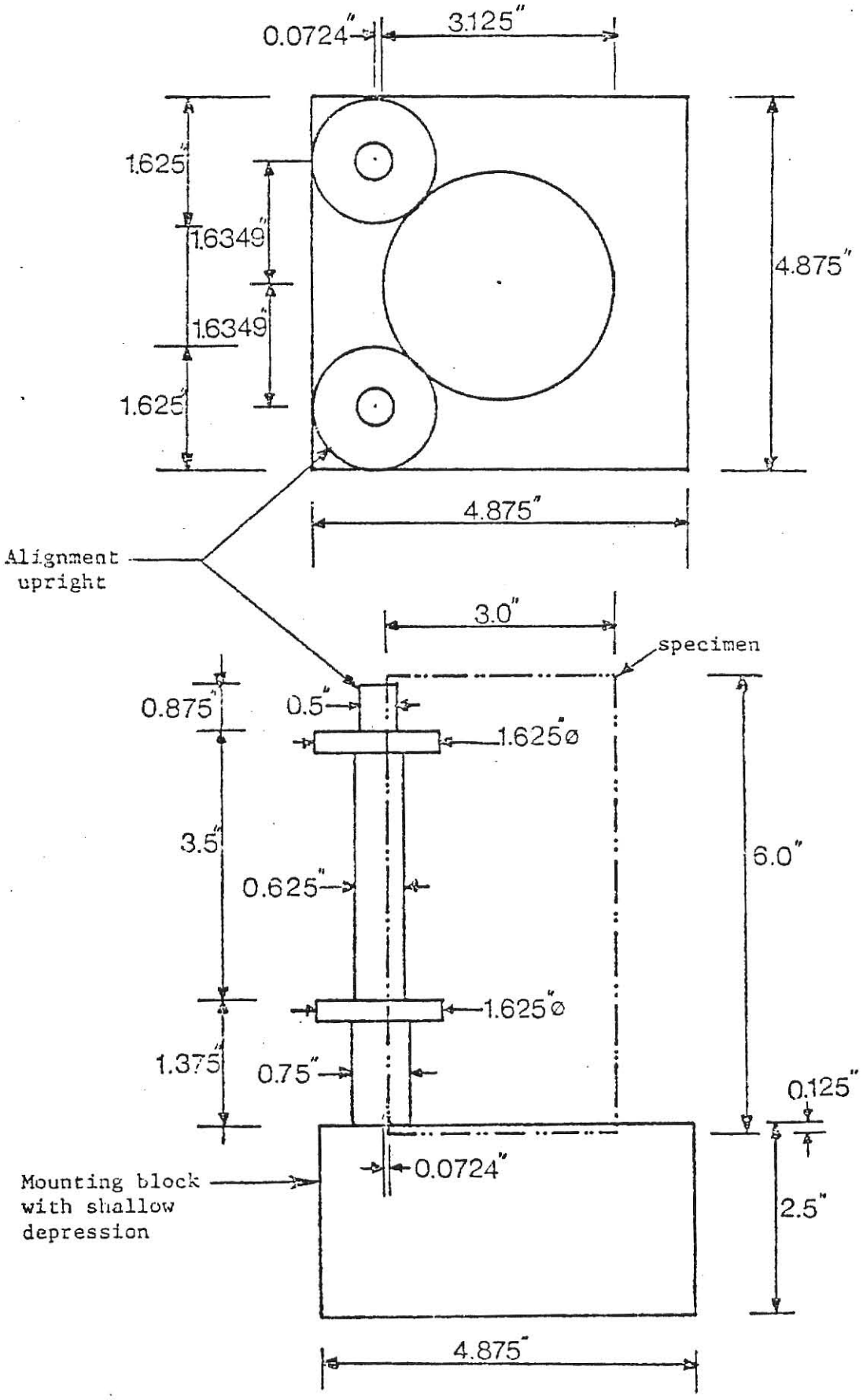

Fig. 2. Tensile Specimen Alignment Jig

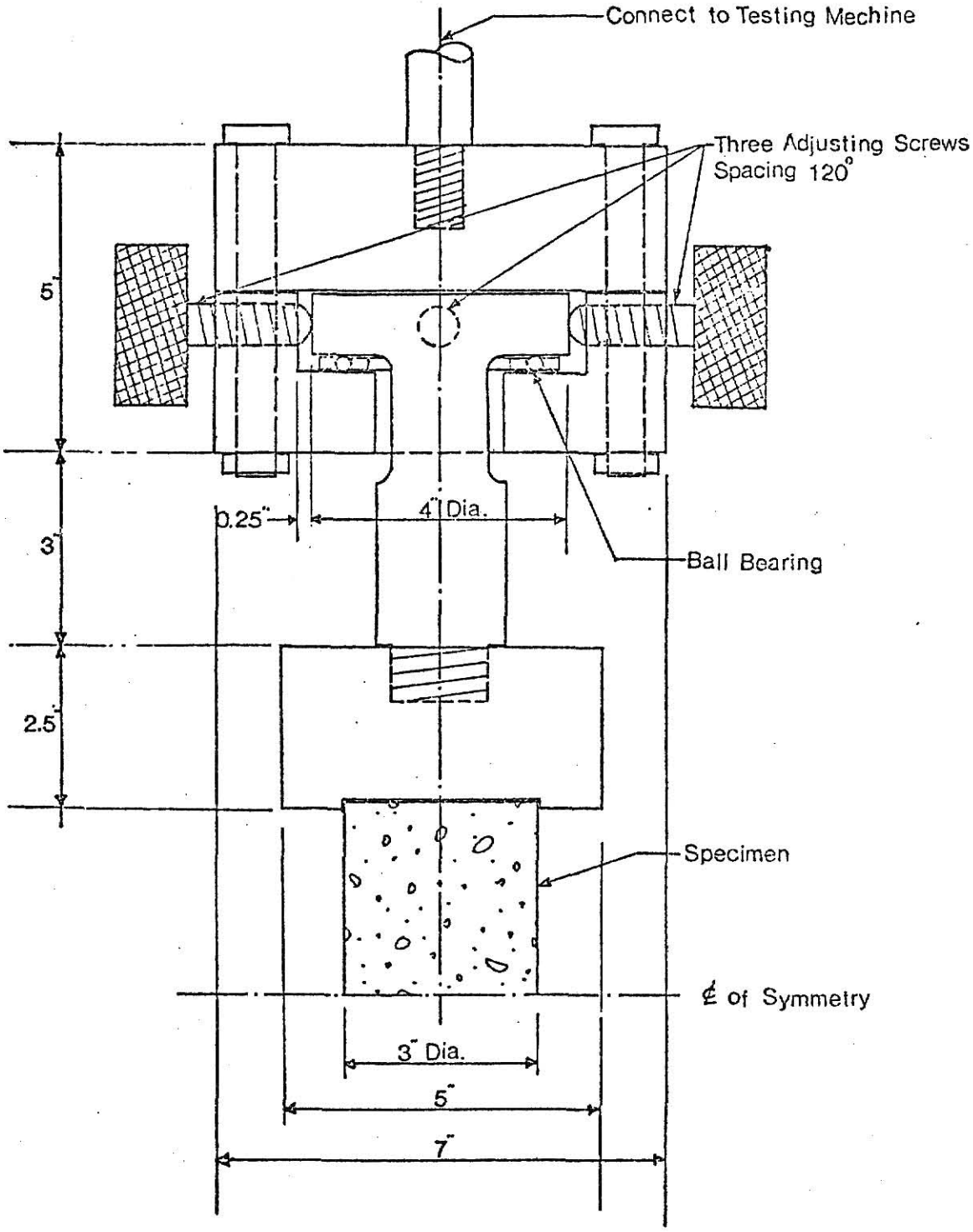

Fig. 3 Tensile Testing Grip

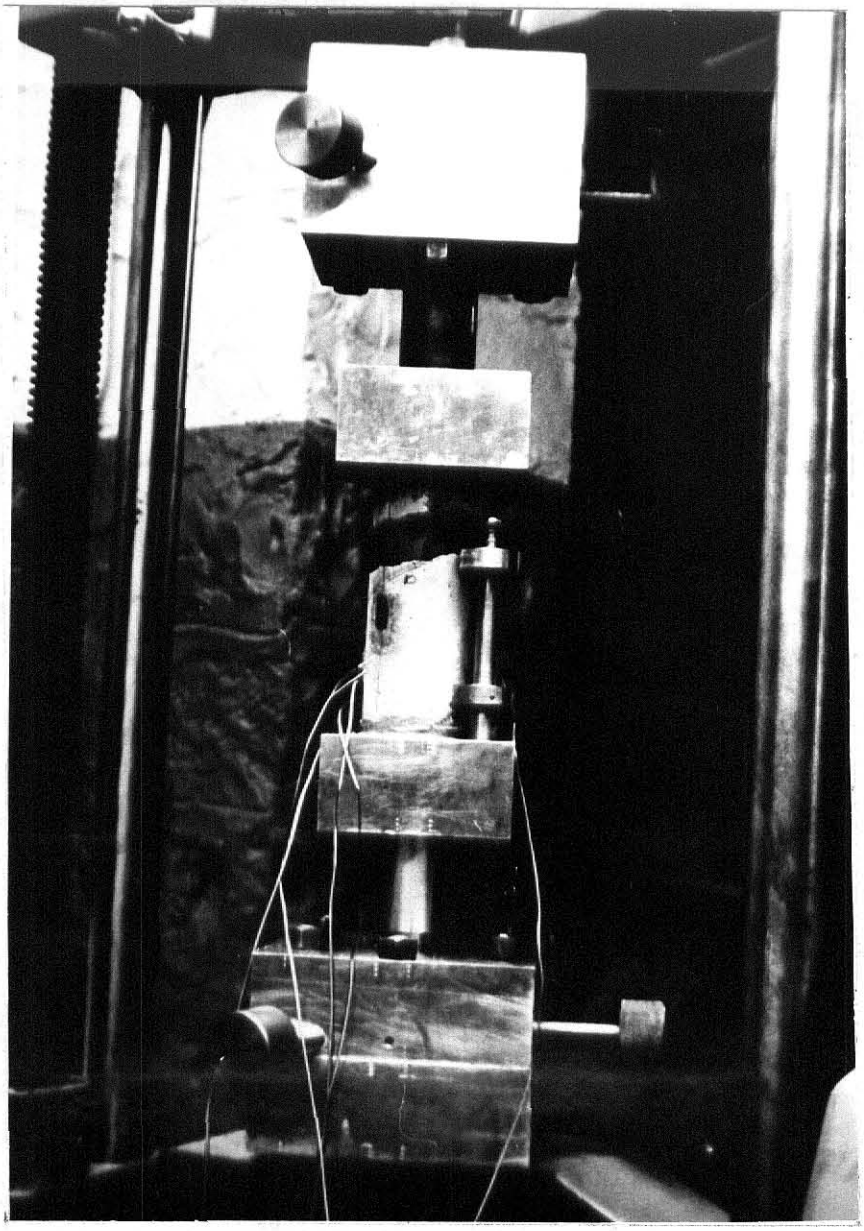

Fig. 4: Tensile Test Setup With Failed Specimen

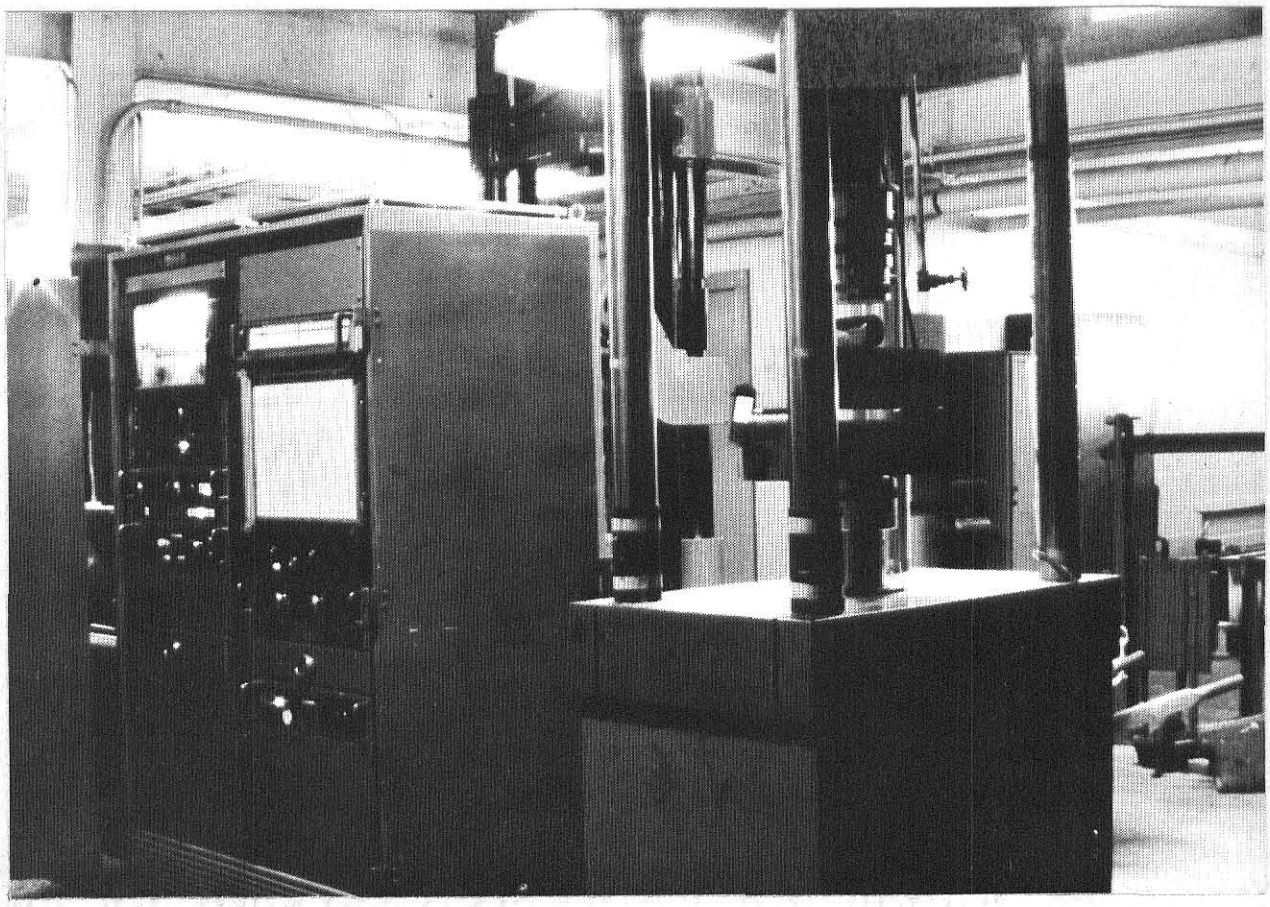

Fig. 5: Test Setup

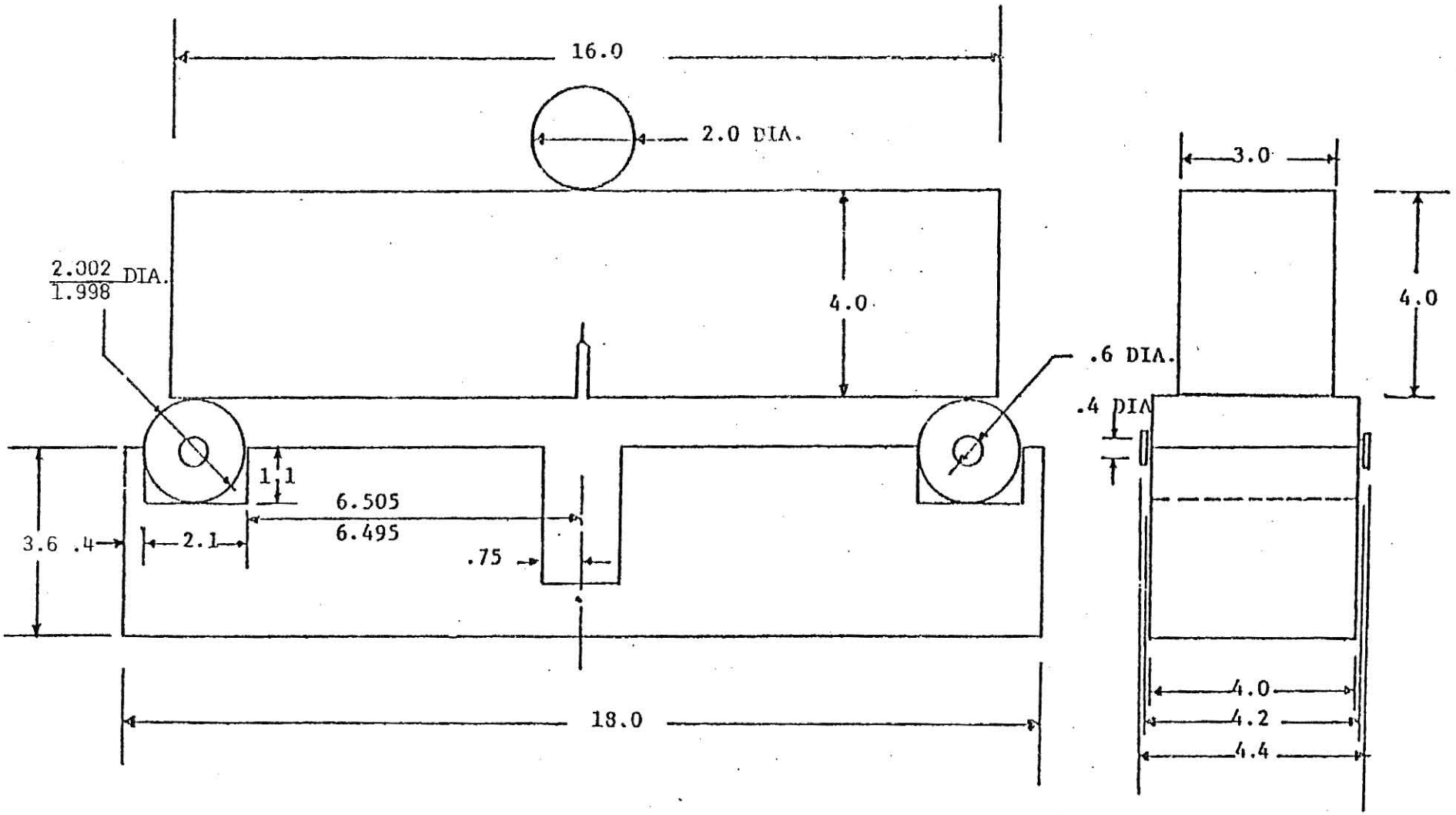

All Dimensions In Inches. 1 in. = 2.54 cm.

Fig. 6: Test Fixture and Specimen Dimensions

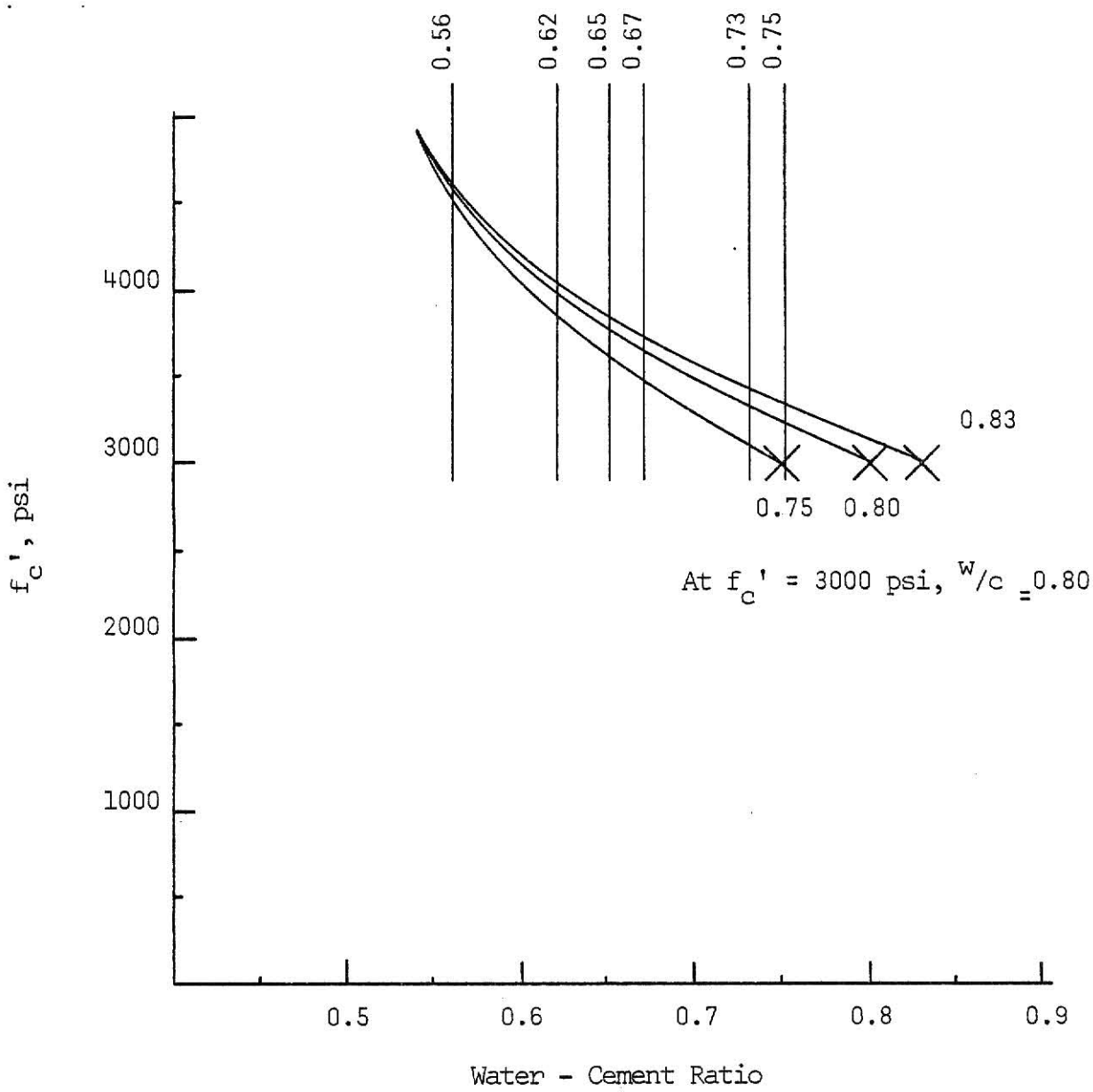

Figure 7. Cylinder Strength Versus Water - Cement Ratio for Trial Mix Design..

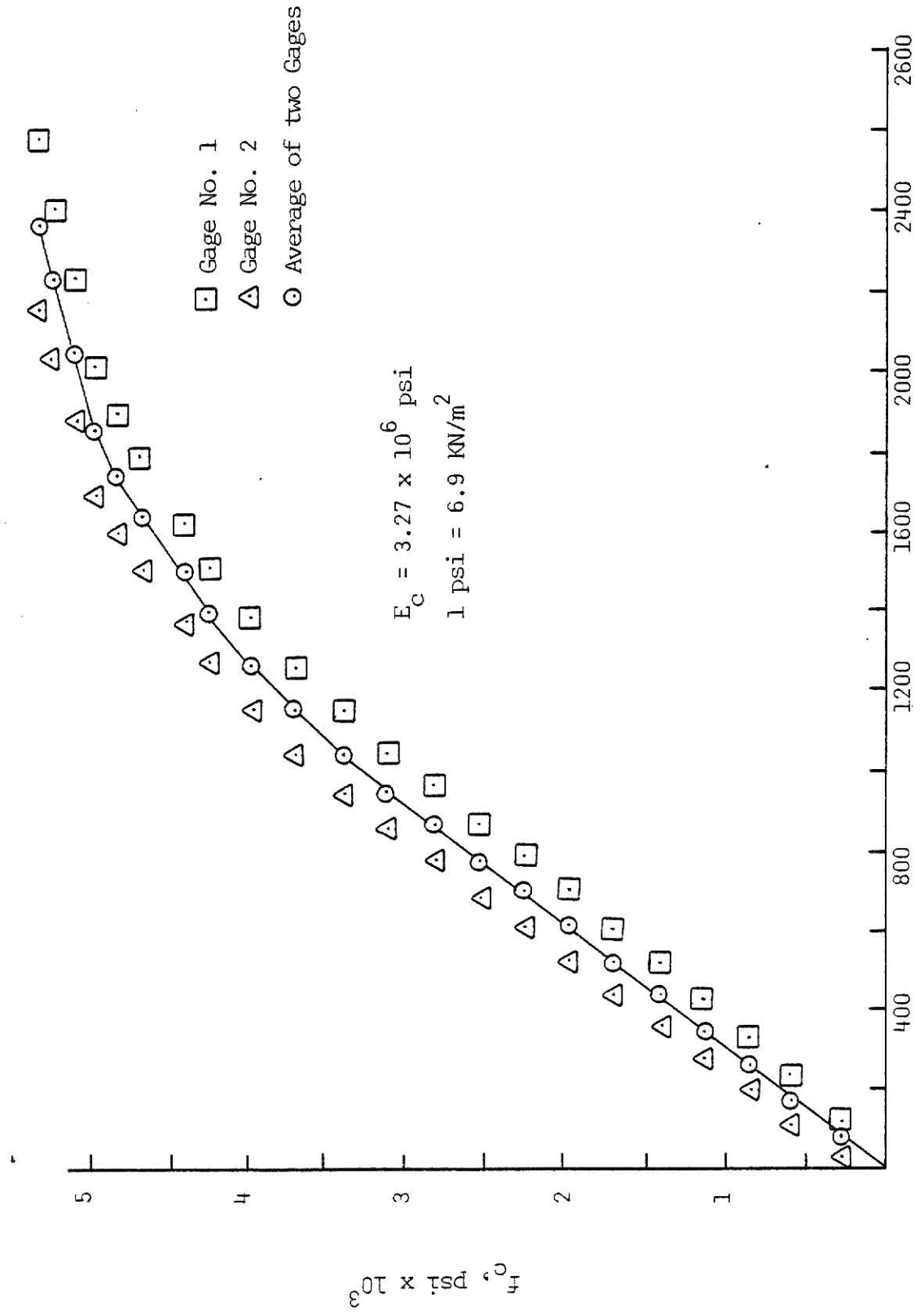

Figure 8: Stress Versus Strain-Compression Cylinder No. 2

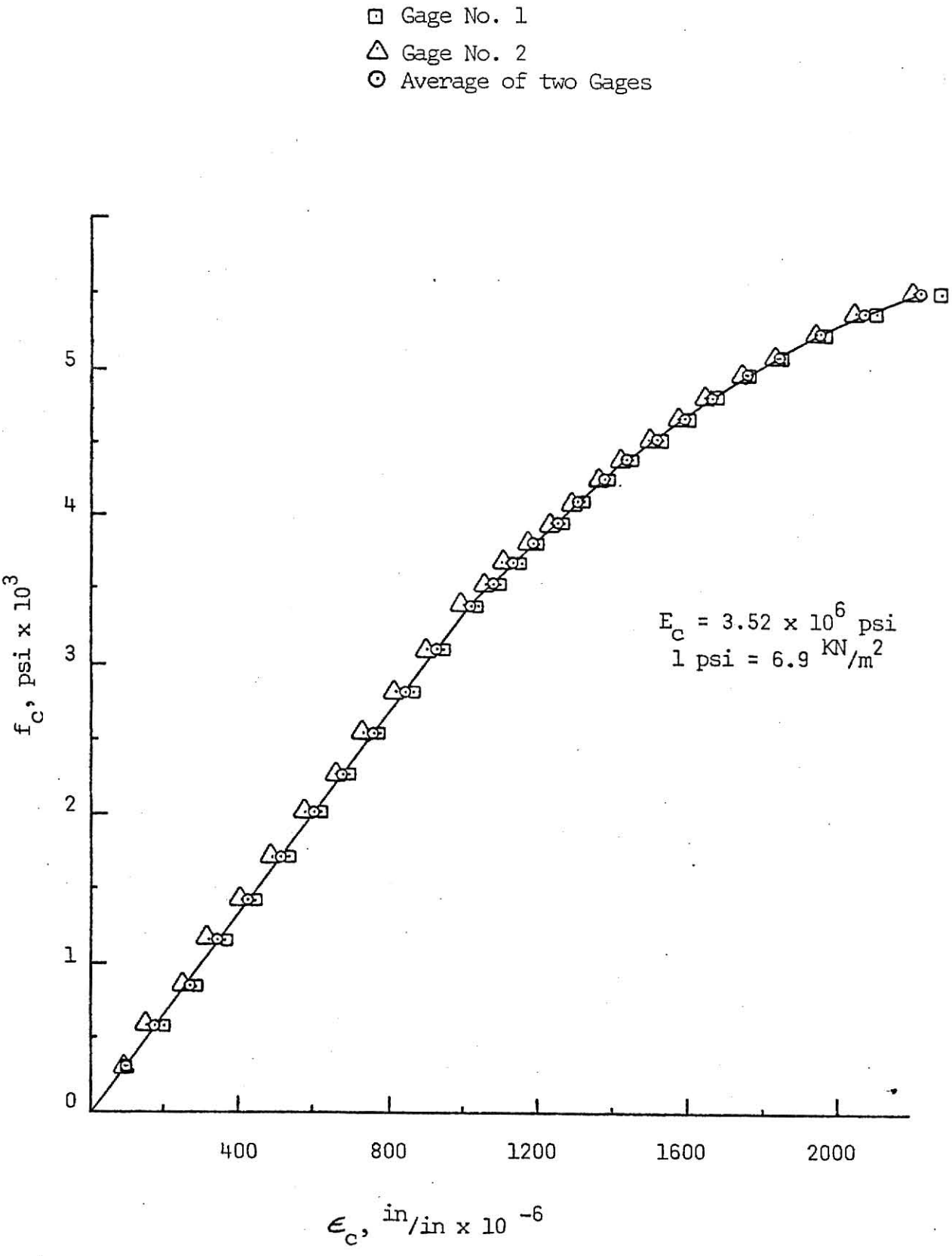

Figure 9. Stress Versus Strain-Compression
Cylinder No. 3

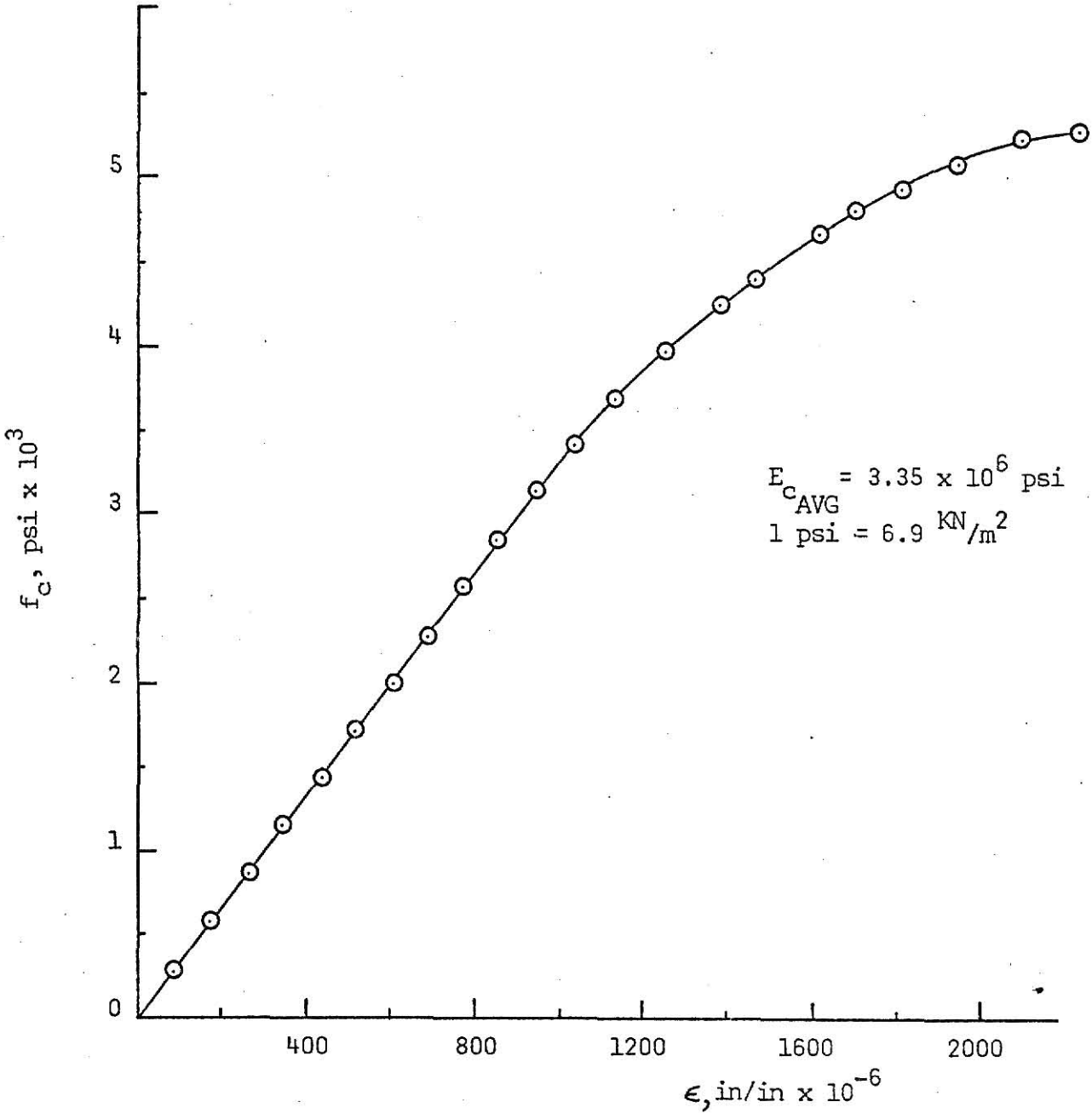

Figure 10. Average Stress Versus Strain for Compression Cylinder Nos. 2 and 3.

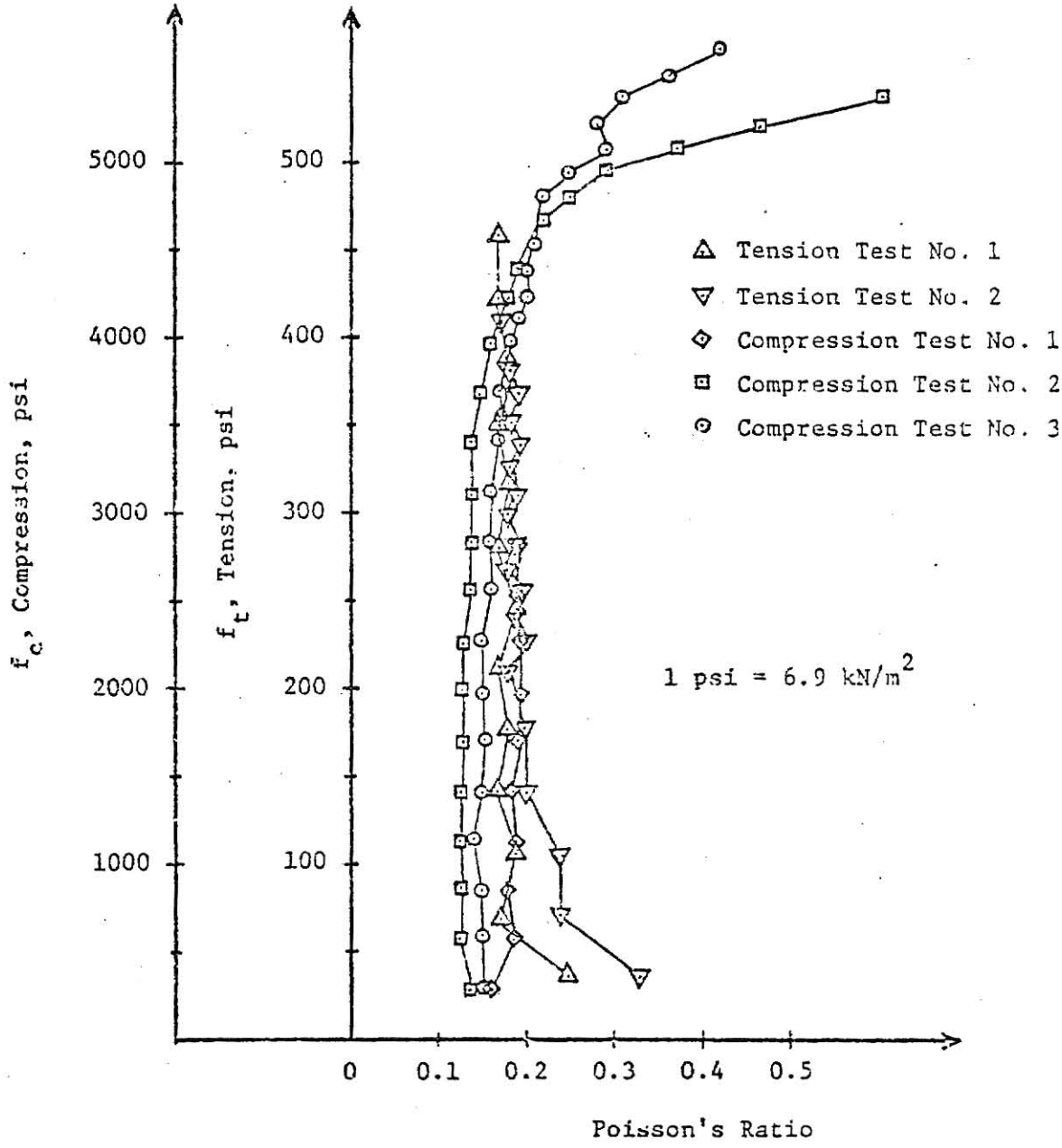

Fig. 11. Stress Versus Poisson's Ratio - All Cylinders

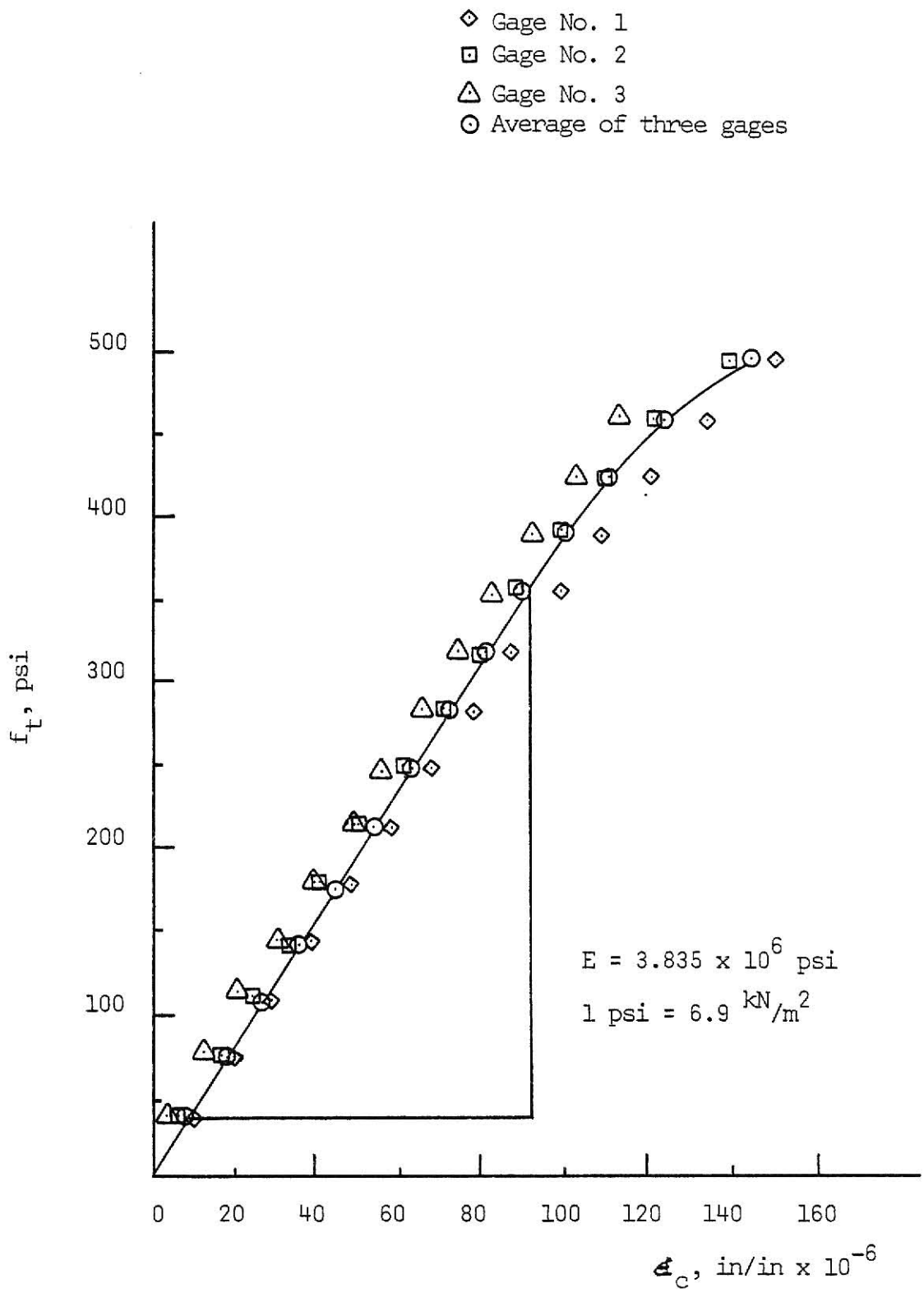

Fig. 12. Tensile Stress Versus Strain-Specimen No. 1.

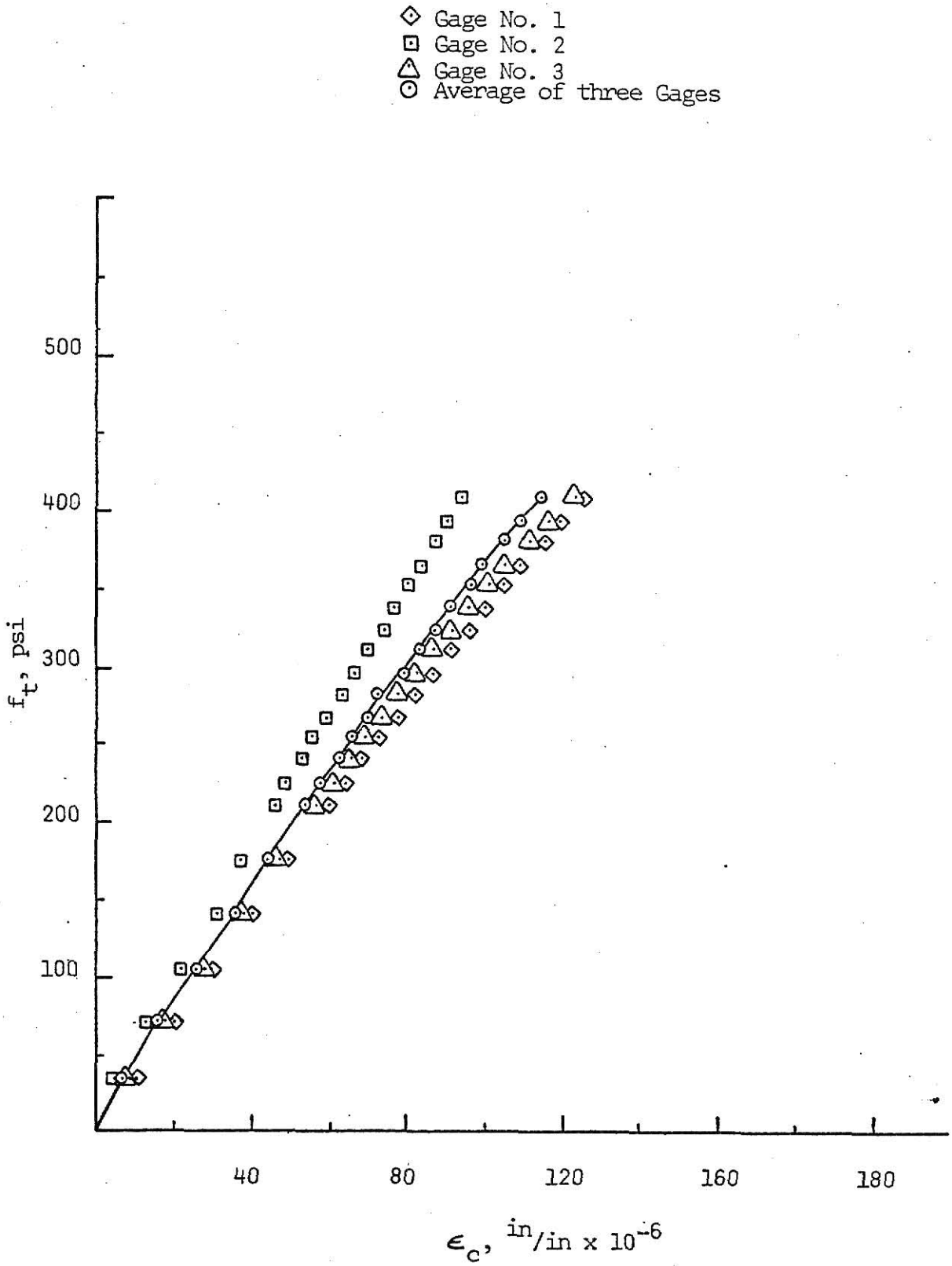

Figure 13. Tensile Stress Versus Strain - Specimen No. 2

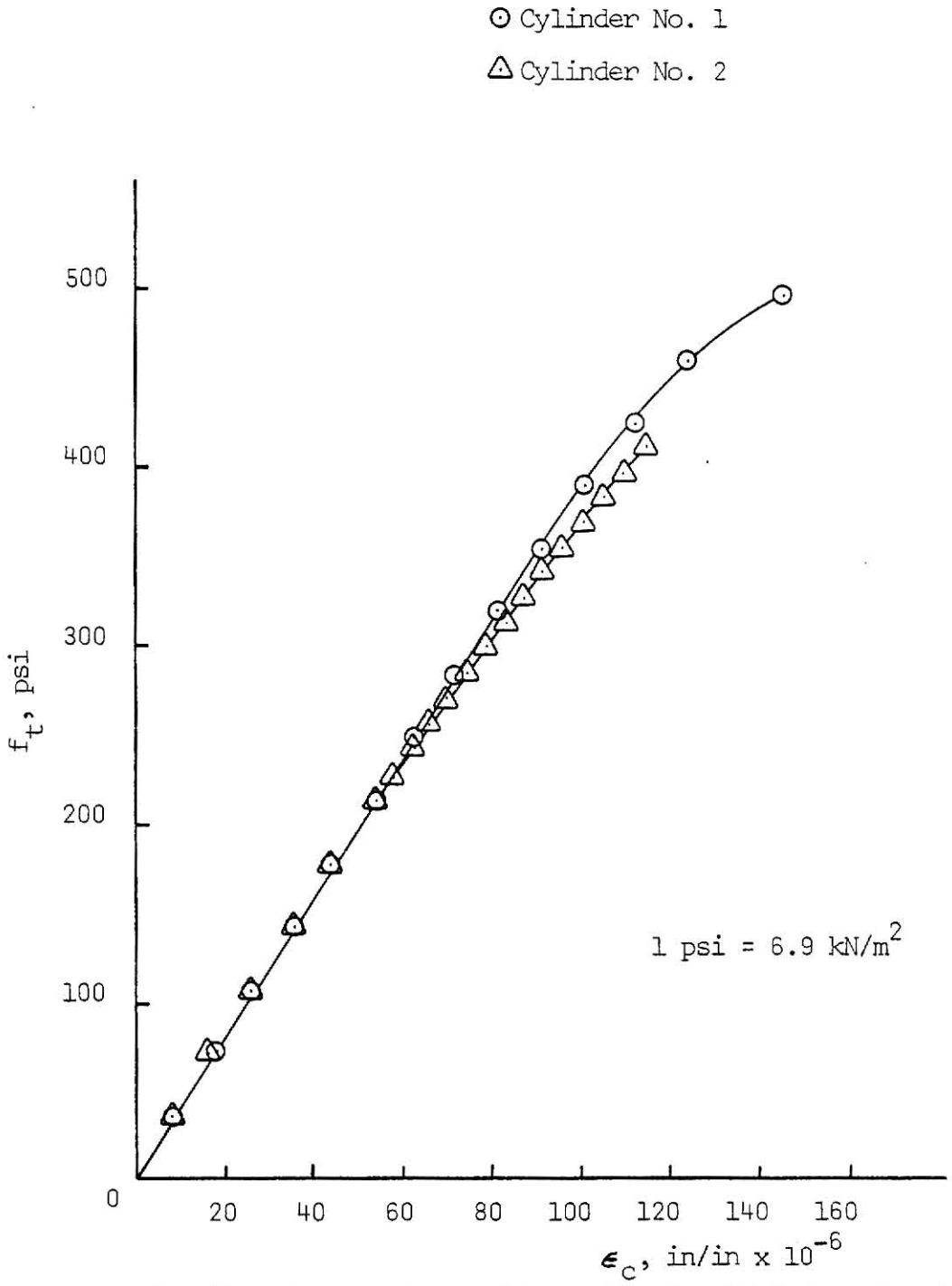

Fig. 14. Average Stress Versus Strain, Cylinders 1 and 2

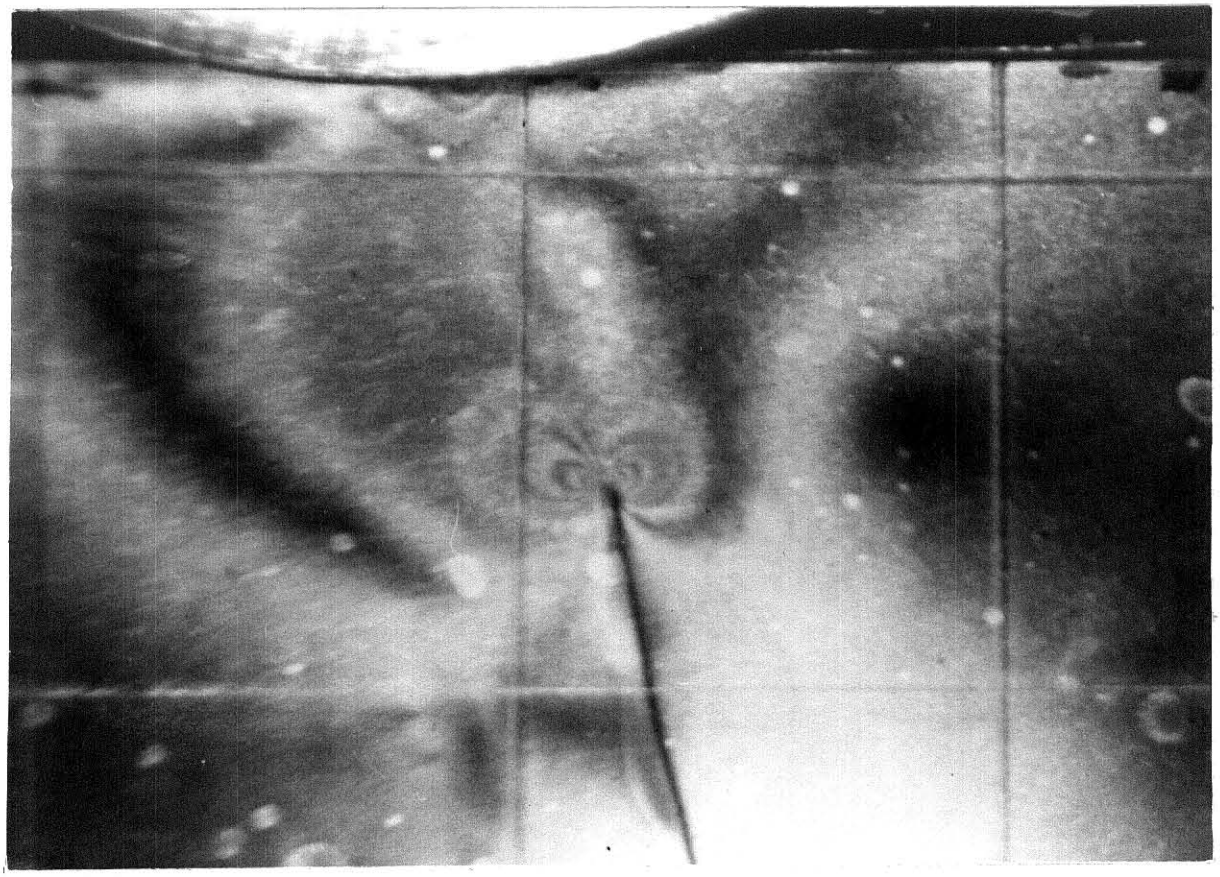

Figure 15. Photoelastic Fringe Pattern Showing the Dissipation of Strain Away From the Crack

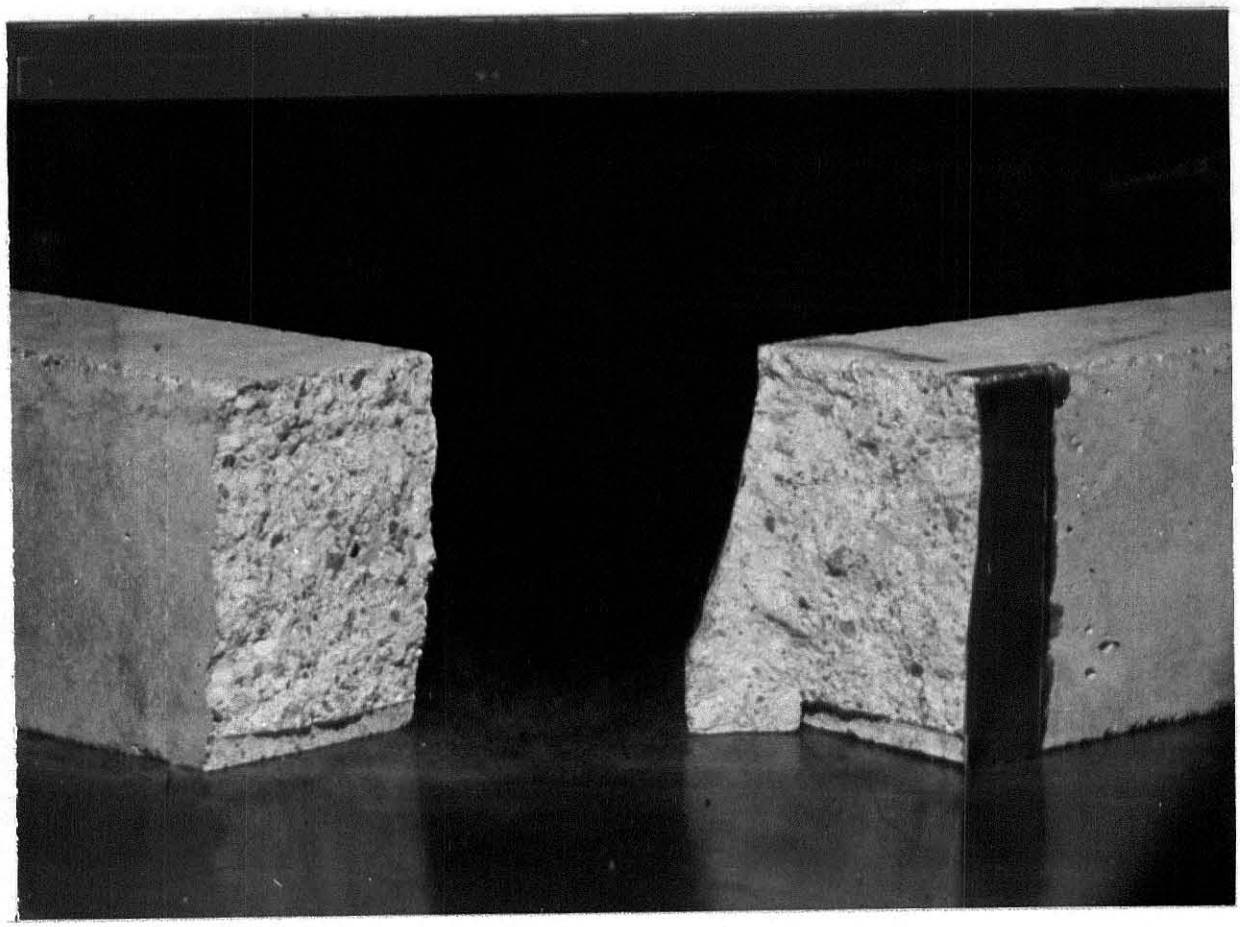

Figure 16. Reinforcing Action of the Photoelastic Sheet.

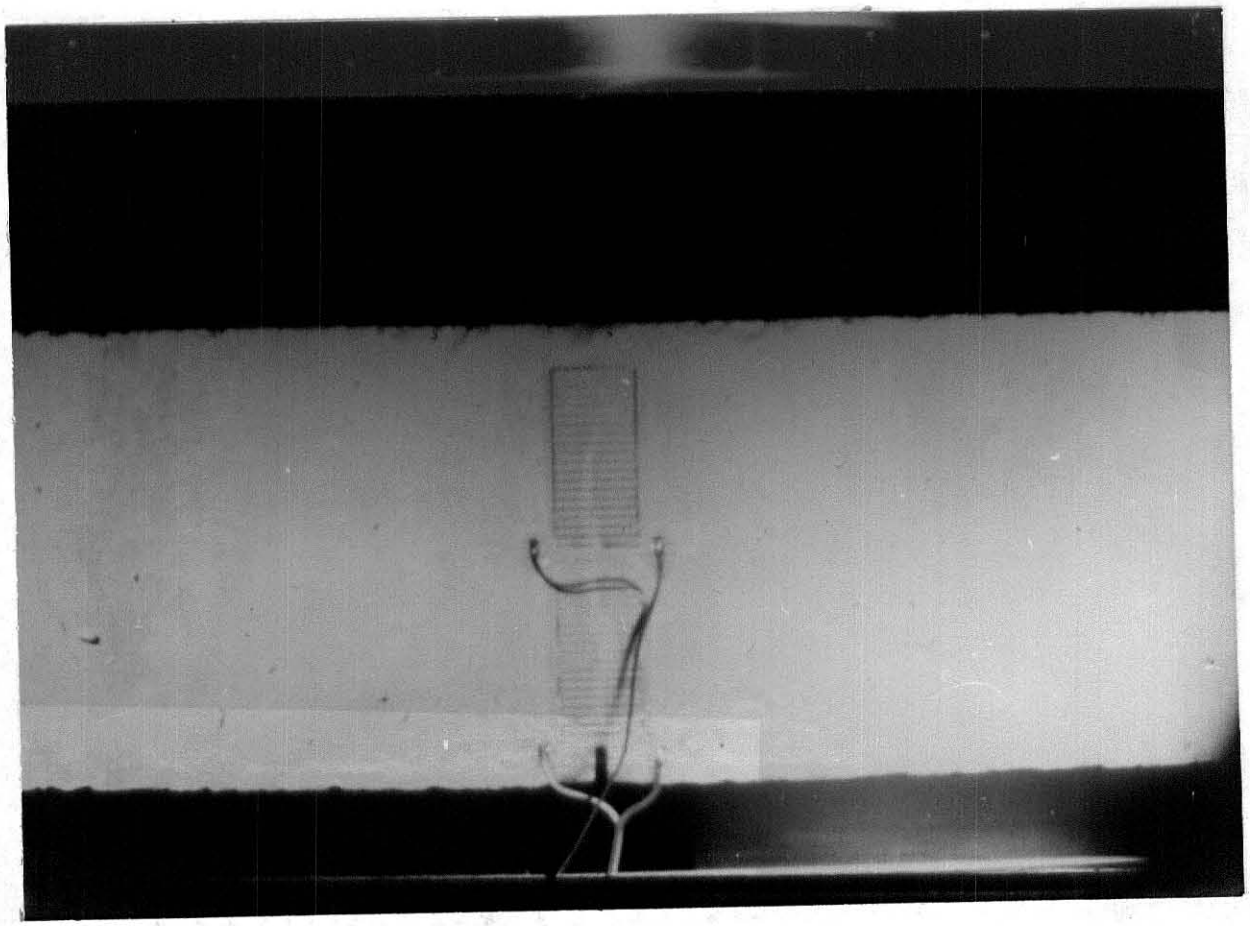

Figure 17. Wire Crack Propagation Gage Mounted on a Specimen.

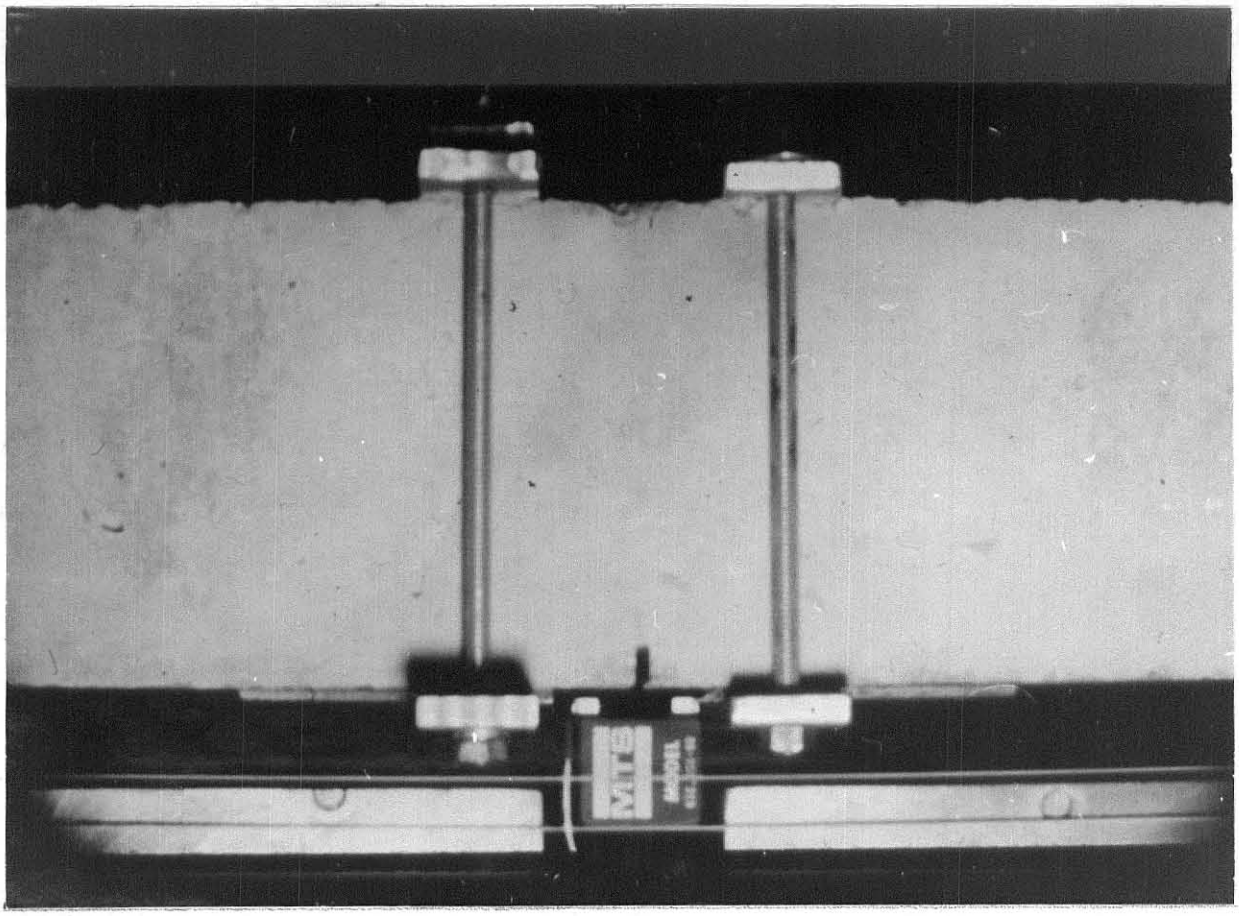

Figure 18. MTS Displaement Gage and Adjustment Clamps.

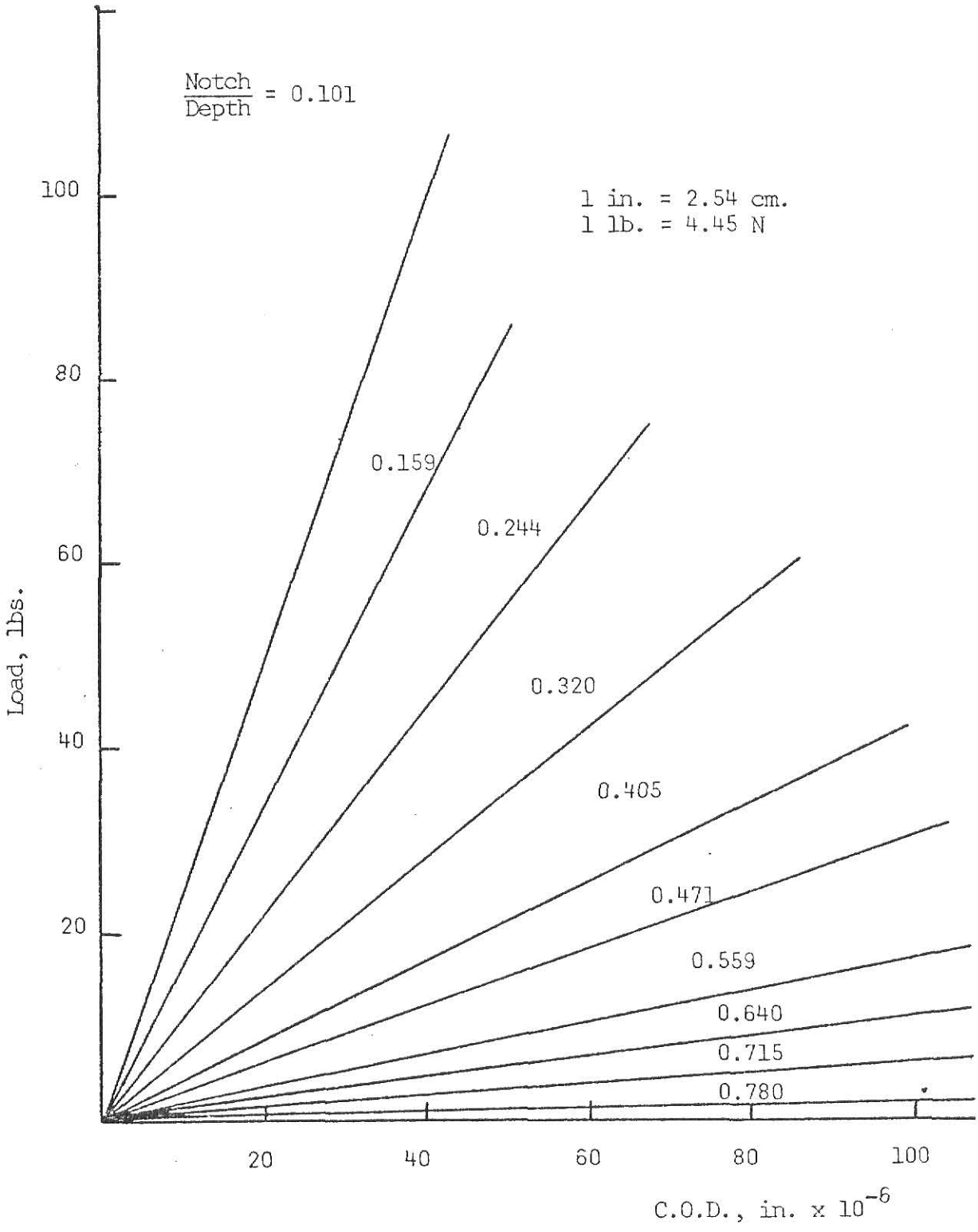

Fig. 19: Load Versus Crack-Opening-Displacement for Compliance Beam

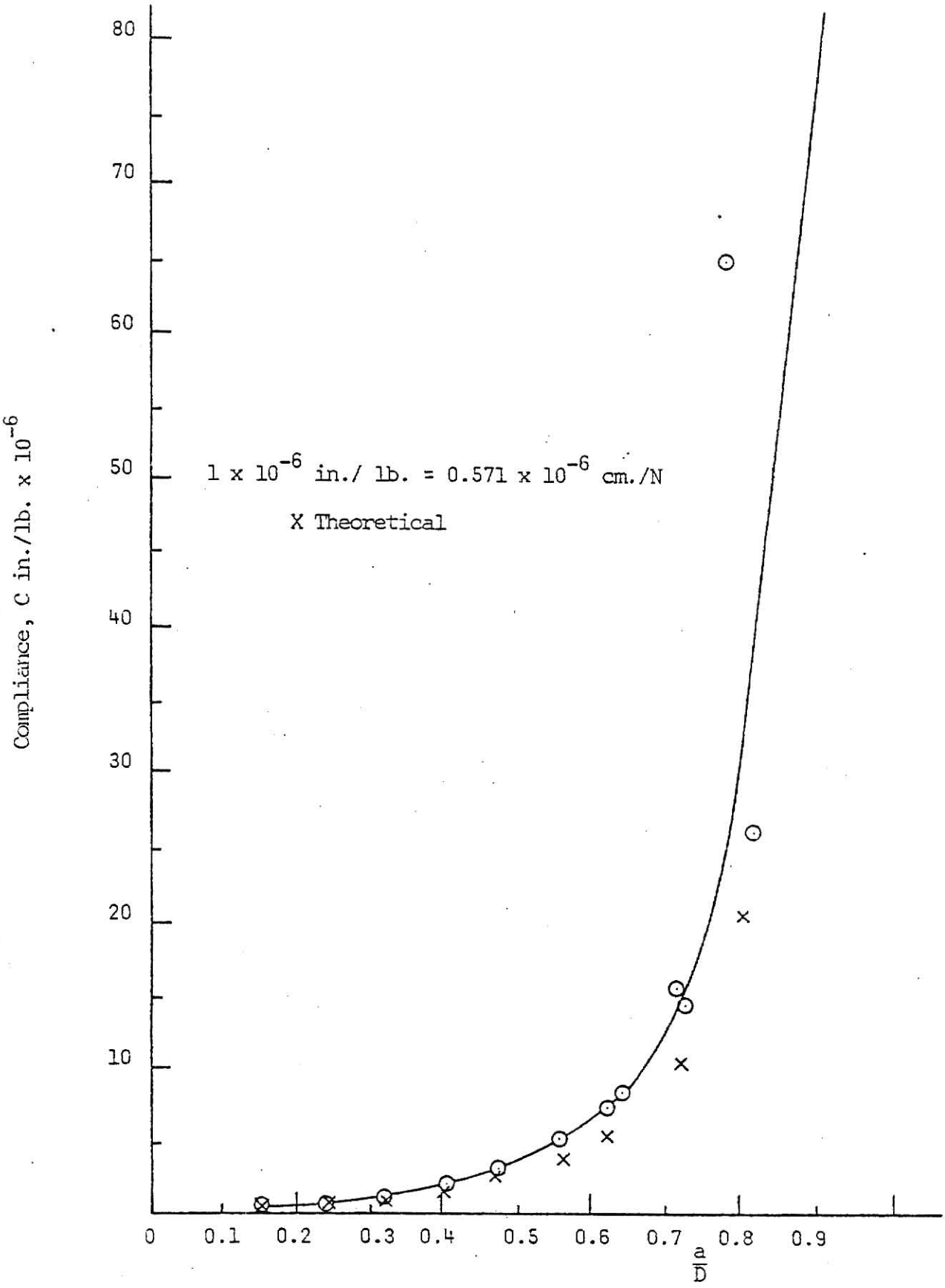

Fig. 20: Compliance Calibration Curve

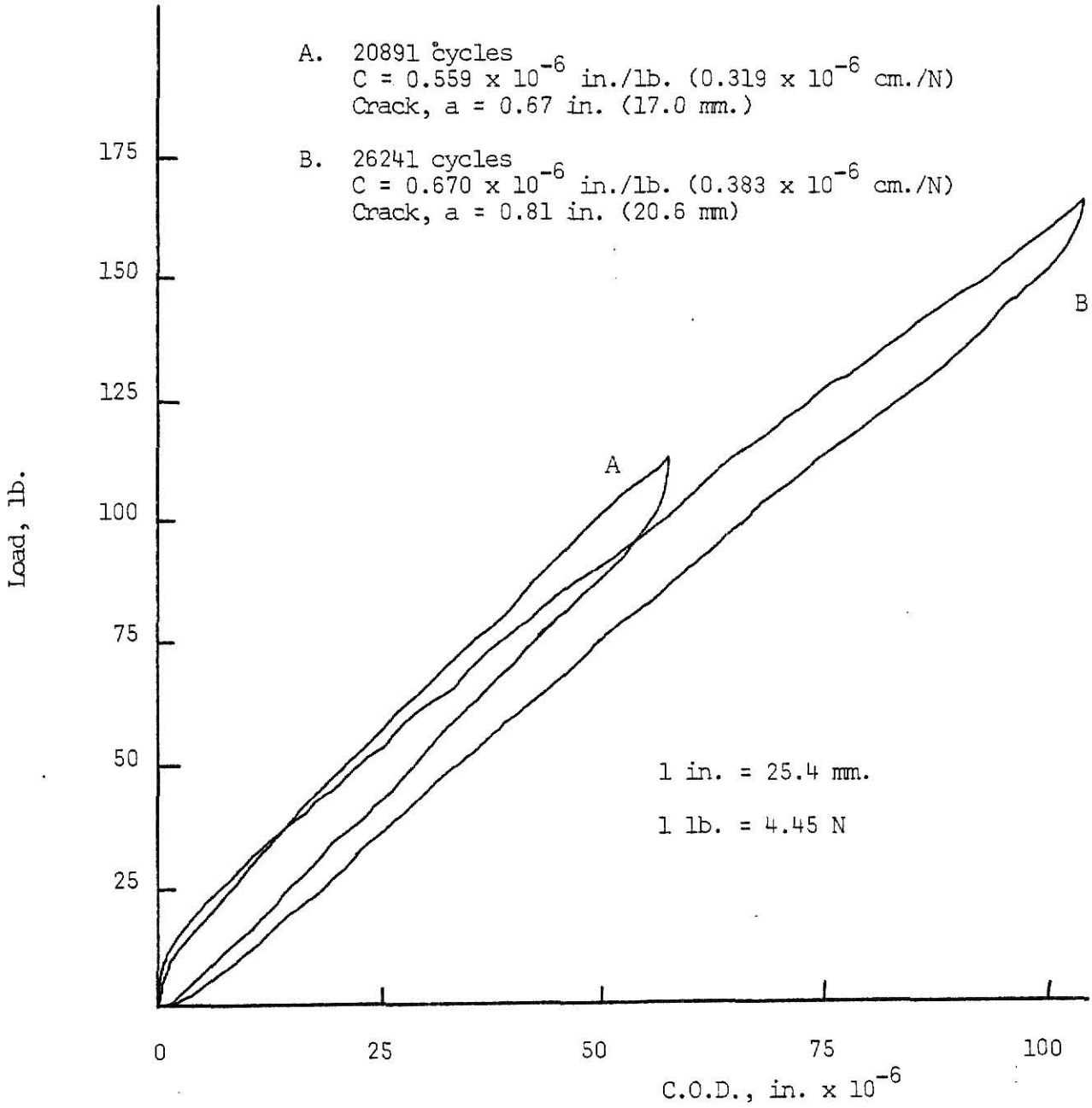

Fig. 21: Load Versus Crack-Opening-Displacement for Beam Cracked in Fatigue-Crack Not Closed, Beam No. 7

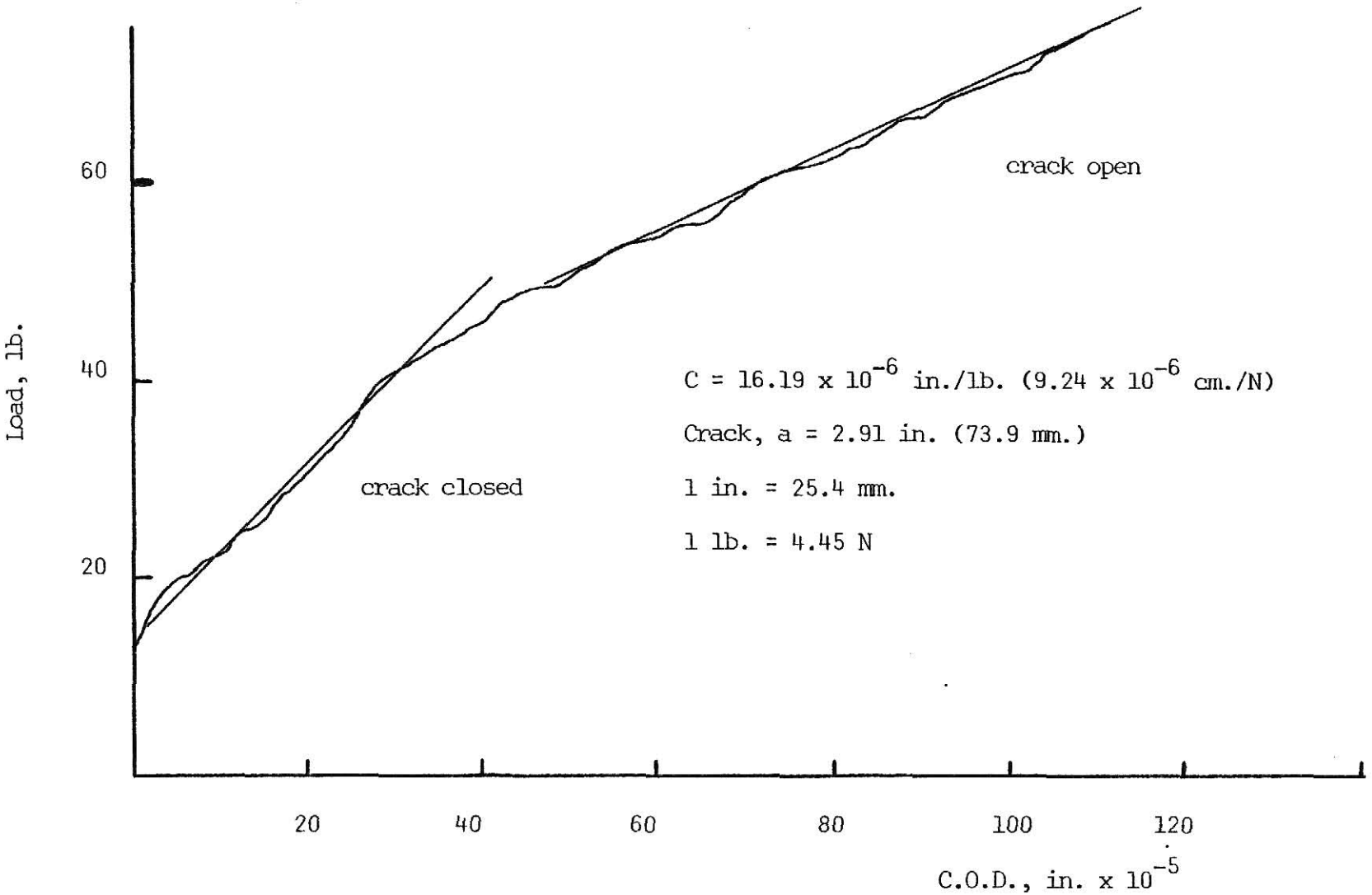

Fig. 22: Load Versus Crack-Opening Displacement for Beam Cracked in Fatigue - Crack Closed Beam No. 5

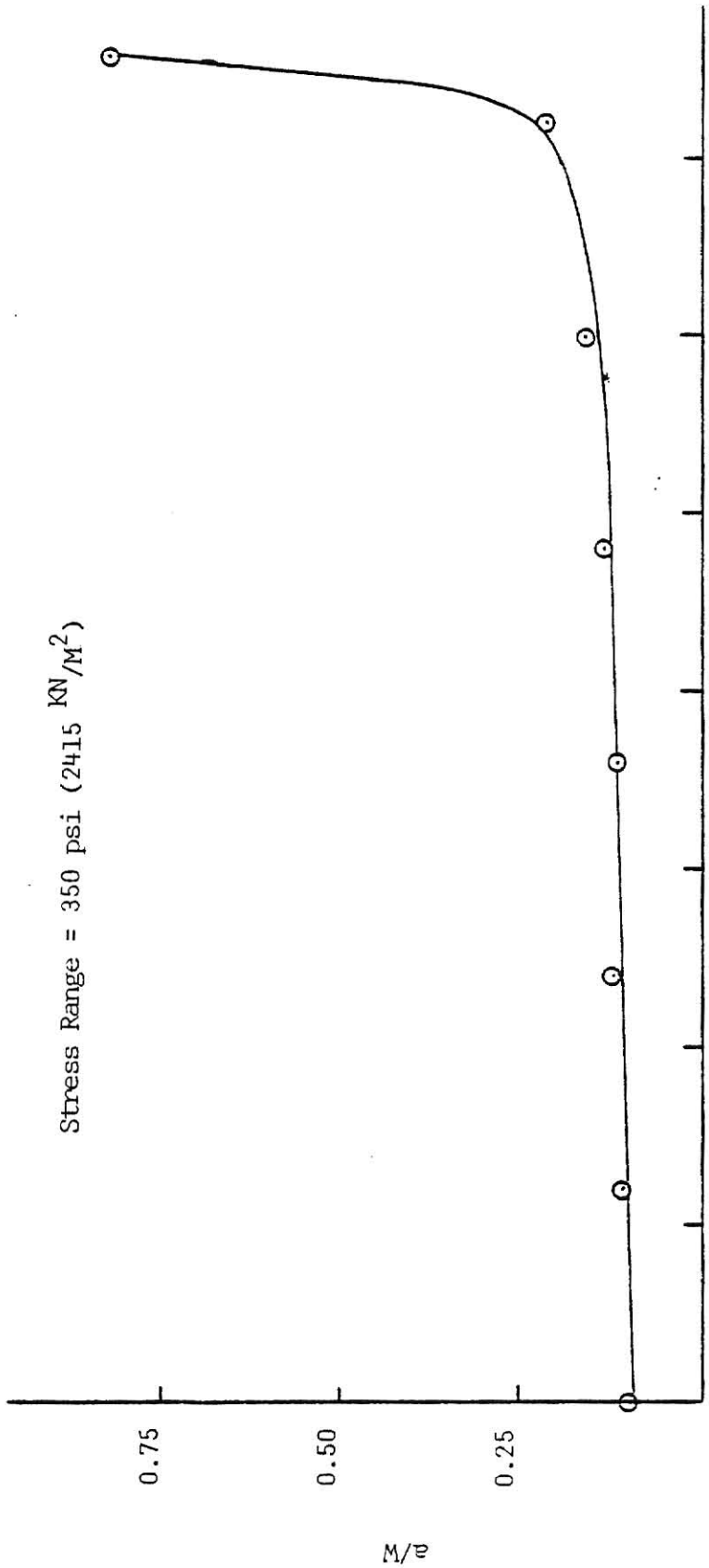

Fig. 23: Crack Growth Versus Load Cycles

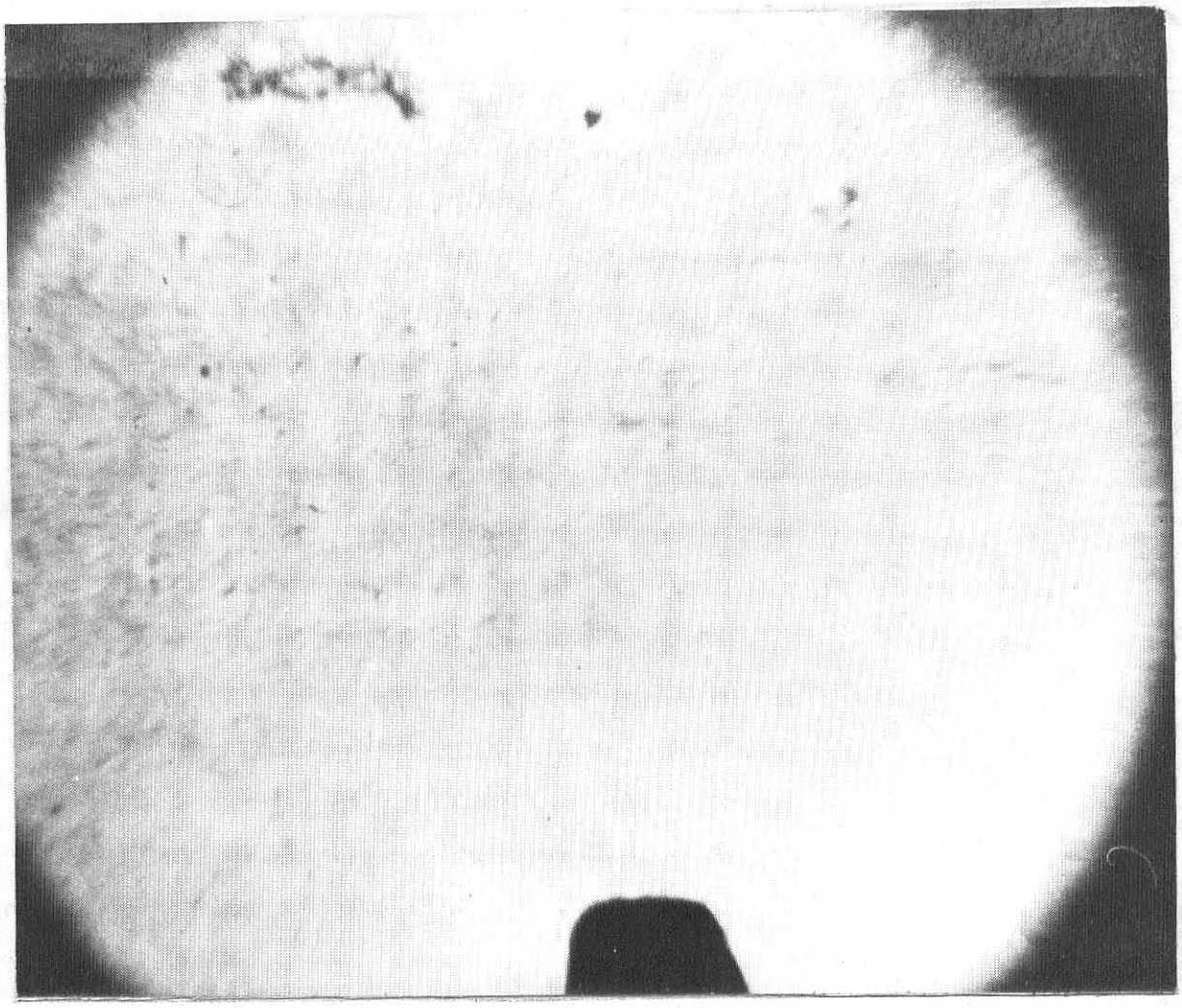

Figure 24:
Beam No. 1 With Fatigue Crack After 8000 Cycles of Load

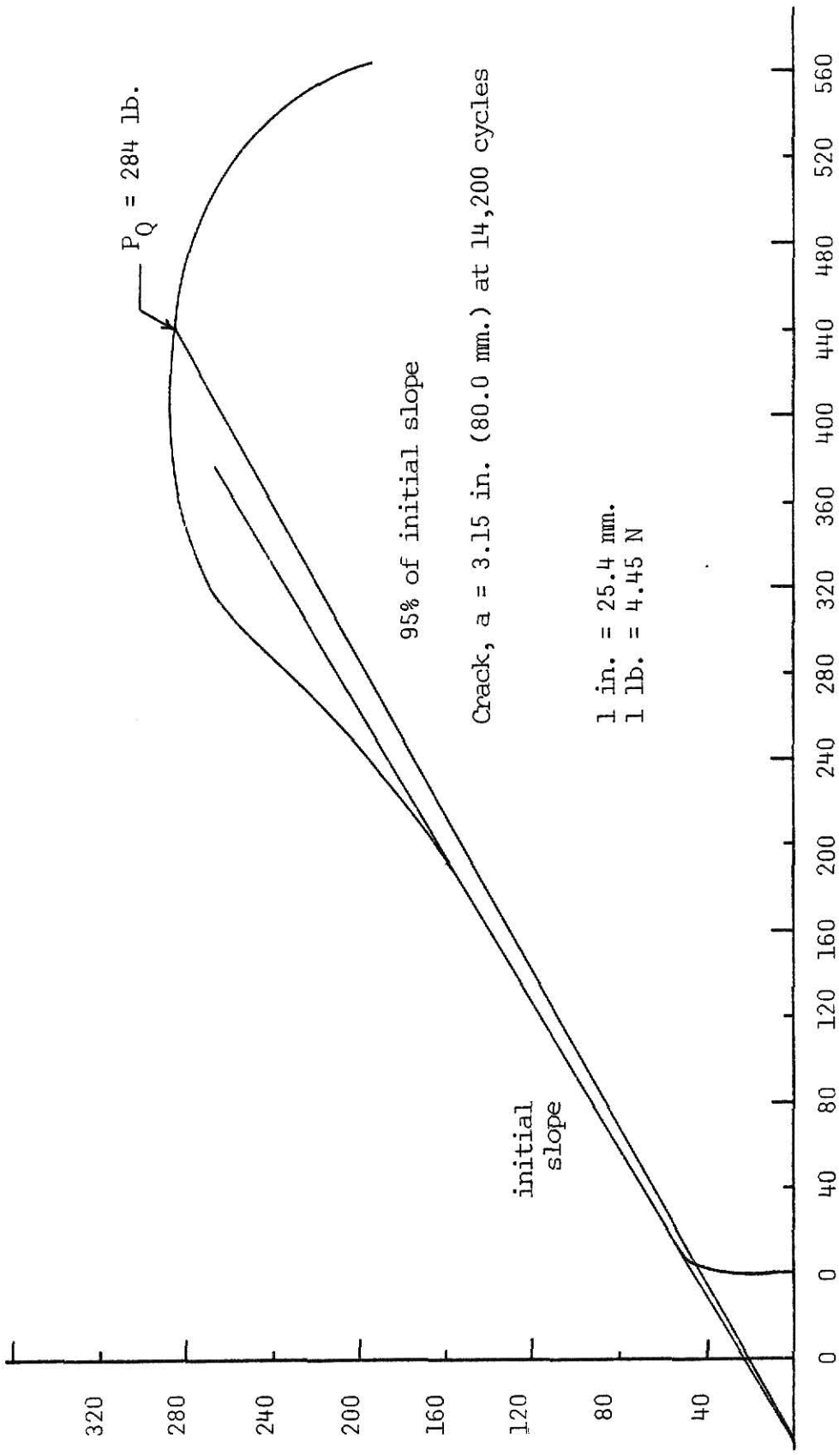

Fig. 25: Load Versus Crack-Opening-Displacement for Pre-Cracked Beam Loaded to Failure Beam No. 6

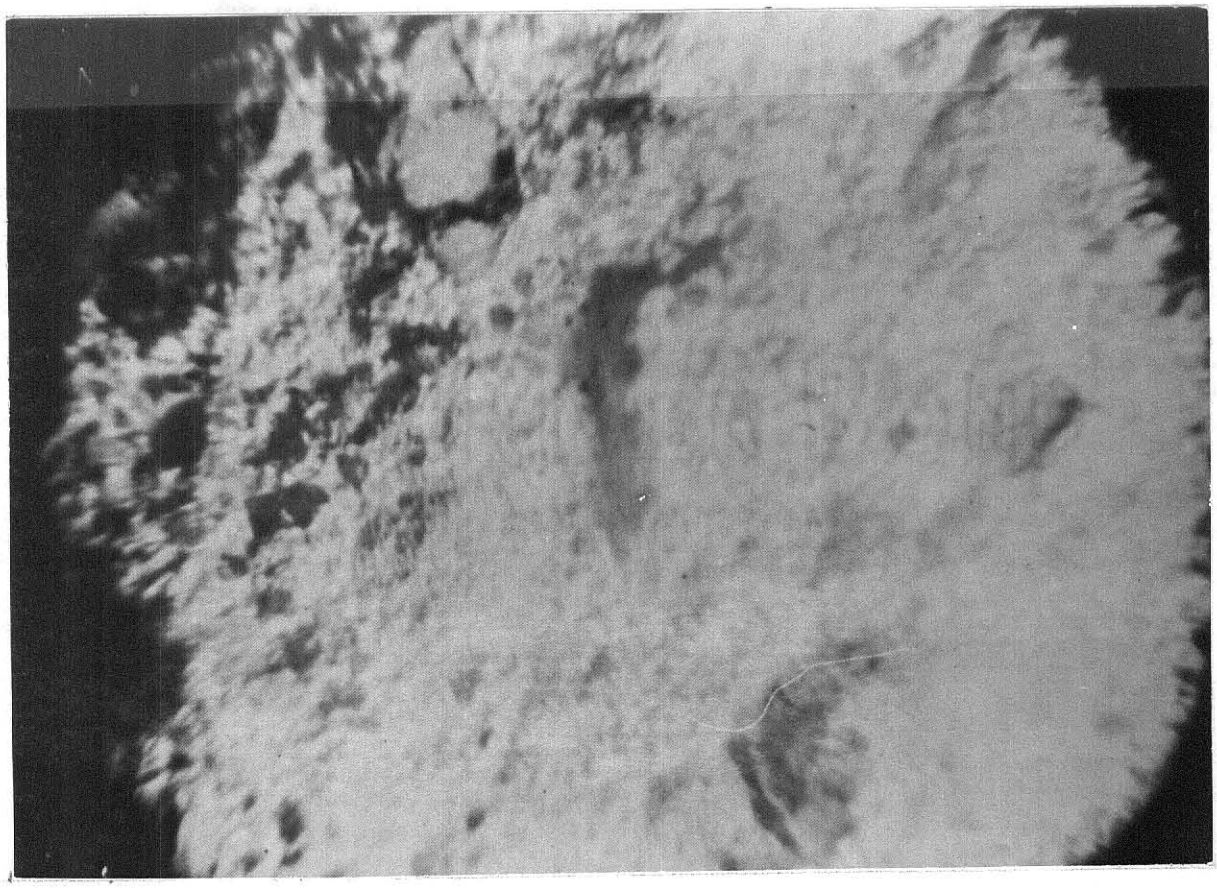

Figure 26: Fracture Appearance of Failed Beam

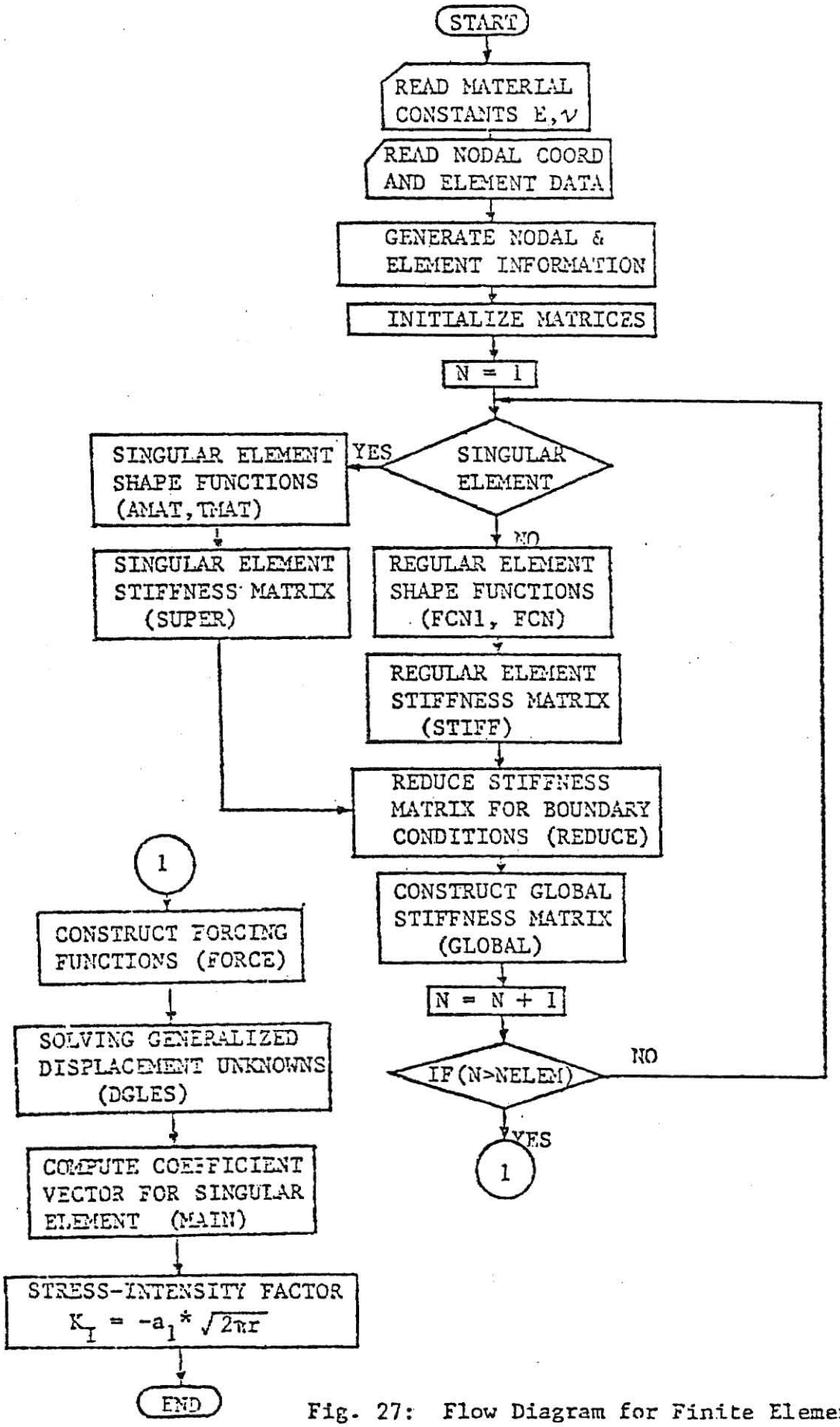

Fig. 27: Flow Diagram for Finite Element Computer Program

Acknowledgements

The writer wishes to thank Dr. Stuart E. Swartz, Professor of Civil Engineering, for his assistance during the research and preparation of this thesis. Sincere thanks is also extended to Dr. Swartz for the encouragement he provided in the time interval between the completion of the research and the completion of this thesis.

Thanks are also extended to Dr. K. K. Hu and James Huang for their valuable assistance in the laboratory and also the preparation of the finite element program used herein. Thanks also to Dr. Robert Snell, Head, Department of Civil Engineering for his continual support during all phases of the project and to the Department of Civil Engineering for providing the facilities.

Special appreciation is due Mr. Russell L. Gillespie for his help in the Civil Engineering Design Shop. Mr. Gillespie provided much valuable help in the fabrication of test fixture and also in the repair of the MTS system.

Finally special thanks and appreciation are extended to the author's family for the valuable encouragement they provided during the period of time between the completion of the research and the completion of this thesis.

Bibliography

1. Brown, W. F., Jr. and Srawley, J. E., "Plane Strain Crack Toughness Testing of High Strength Metallic Materials," ASTM STP41D, ASTM, Philadelphia, 1966.

2. Glücklich, Joseph, "Fracture of Plain Concrete," Journal of the Engineering Mechanics Division, ASCE, Vol. 89, No. EM6, Part 1, Proc. Paper 3715, Dec. 1963, pp. 127-138.

3. Huang, Chen-Ming James, "Finite Element and Experimental Studies of Stress-Intensity Factors for Concrete Beams," dissertation submitted to Kansas State University in partial fulfillment of the requirements for the degree Doctor of Philosophy, Manhattan, Kansas, 1981.

4. Naus, Dan J. and Lott, James L., "Fracture Toughness of Portland Cement Concretes," Journal of the American Concrete Institute, No. 6, Proceedings V. 6, June 1969, pp. 481-489.

5. Schmidt, R. A., "Fracture Toughness Testing of Limestone," Experimental Mechanics, SESA, No. 5, Proceedings V. 16, May 1976.

6. Shah, Surendra P., and McGarry Fred J., "Griffith Fracture Criterion and Concrete," Journal of the Engineering Mechanics Division, ASCE, Vol. 97, No. EM6, Proc. Paper 8597, Dec. 1971, pp. 1663-1676.

CRACK GROWTH MEASUREMENT AND FRACTURE TOUGHNESS OF PLAIN CONCRETE BEAMS

by

Gary Lee Jones
B.S. Kansas State University, 1976

An Abstract of a Master's Thesis

submitted in partial fulfillment of

the requirements for the degree

MASTER OF SCIENCE

Department of Civil Engineering

Kansas State University
Manhattan, Kansas

1982

Abstract

The process of crack growth and propagation in concrete takes place on a level which makes direct determination of crack length virtually impossible. To adequately monitor the cracking process and relate the results to variations in the material properties of concrete, reliable means of crack growth determinations must be devised.

This thesis examines photoelasticity, crack propagations gages, visual inspection, and compliance for suitability as methods for monitoring crack propagation. Experimental results indicated that photoelasticity was not an acceptable method. Compliance proved to produce accurate results and visual inspection, when used in conjunction with compliance, also yielded accurate results. Crack propagation gages, as used in experiments for the thesis, were inadequate but results tended to indicate that methods might be developed where the gages would yield satisfactory results.

A total of twenty-four 3 in. x 4 in. (7.62 cm x 10.16 cm) beams were cast of which eight were used for test results. Thirty 3 in. x 6 in. (7.62 cm x 15.24 cm) test cylinders were cast. Fifteen cylinders were used to monitor the compressive strength stablization and two were used to determine the direct tensile strength of the final mix design.